Cell Reports

Article

Widespread impact of nucleosome remodelers on transcription at *cis*-regulatory elements

Graphical abstract

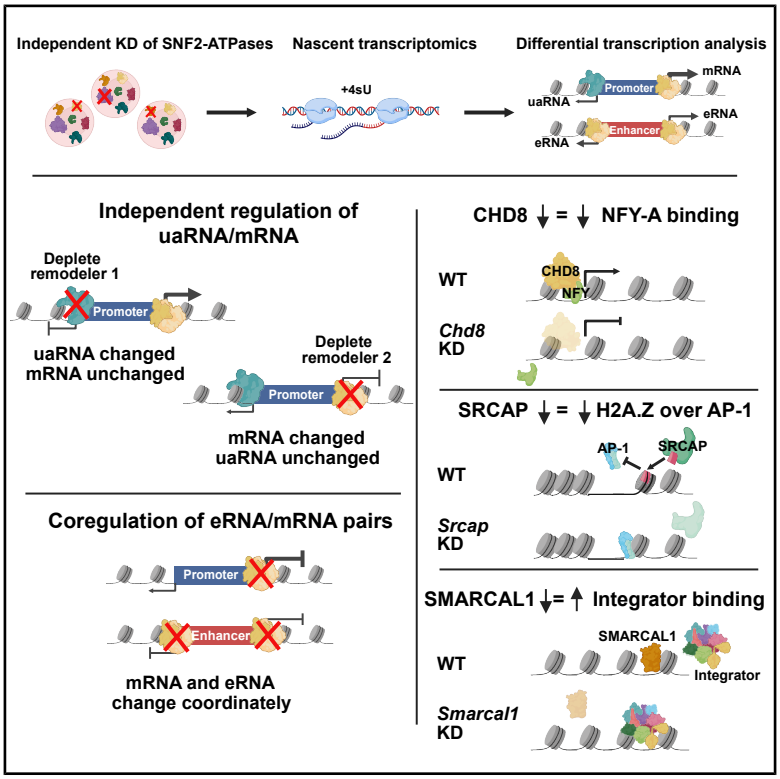

Highlights

- Nascent transcriptomic screen for SNF2-type remodelers in gene regulatory networks
- Transcription of uaRNAs and mRNAs sharing a promoter is not co-regulated by remodelers
- CHD8 functionally interacts with NFYA; SRCAP regulates H2A.Z binding over AP-1 motifs
- SMARCAL1 and remodelers associated with genome stability may act via Integrator activity

Authors

Benjamin J. Patty, Rinku Dhungana, Sarah J. Hainer

Correspondence

sarah.hainer@pitt.edu

In brief

Patty et al. systematically investigate the effects of SNF2 remodelers on *cis*-regulatory element transcription, both coding and non-coding, offering insights into the role of nucleosome remodeling complexes in gene regulatory networks. They define distinct molecular mechanisms for CHD8, SRCAP, and SMARCAL1.

Patty et al., 2025, Cell Reports *44*, 115767
June 24, 2025
https://doi.org/10.1016/j.celrep.2025.115767

CellPress

Cell Reports

CellPress
OPEN ACCESS

Article

Widespread impact of nucleosome remodelers on transcription at *cis*-regulatory elements

Benjamin J. Patty,[1] Rinku Dhungana,[1] and Sarah J. Hainer[1,2,3,*]
[1]Department of Biological Sciences, University of Pittsburgh, Pittsburgh, PA 15213, USA
[2]UPMC Hillman Cancer Center, University of Pittsburgh, Pittsburgh, PA 15213, USA
[3]Lead contact
*Correspondence: sarah.hainer@pitt.edu
https://doi.org/10.1016/j.celrep.2025.115767

SUMMARY

Nucleosome remodelers and regulatory factors collaborate to establish chromatin environments that control gene expression through *cis*-regulatory elements (CREs) such as promoters and enhancers, which drive transcription of mRNAs and CRE-associated non-coding RNAs (ncRNAs). Two CRE-associated ncRNAs include upstream antisense RNAs (uaRNAs) and enhancer RNAs (eRNAs). The role of remodelers in regulating CRE activity remains incompletely understood. Here, we investigated how SNF2-family remodelers regulate mRNA, eRNA, and uaRNA transcription in murine embryonic stem cells. We identified thousands of misregulated transcripts upon remodeler depletion and defined contributions of understudied remodelers. We find that paired mRNAs and eRNAs are co-regulated, while mRNAs and uaRNAs sharing a promoter are independently regulated by remodelers. Mechanistic studies reveal that CHD8 and SRCAP modulate transcription through canonical transcription factor and histone variant mechanisms, while other remodelers, including SMARCAL1, impact transcription indirectly by maintaining genomic stability. Our findings define classes of SNF2 remodelers in regulating the CRE-associated transcriptome.

INTRODUCTION

Nucleosome remodeling complexes (remodelers) serve critical roles in DNA-templated processes, including transcription, replication, and DNA repair.[1–4] Remodelers are highly diversified in eukaryotic systems, with at least 32 SNF2-like ATPase proteins, many of which are classified into four subfamilies (SWI/SNF, INO80, ISWI, and CHD) based on the presence of subfamily-specific protein domains within the catalytic subunit.[1,2] A subset of these SNF2-like proteins lack these defining domains and are currently sorted into a less well-defined outgroup.[1,2] Remodelers utilize ATP hydrolysis to translocate DNA, resulting in nucleosome mobilization through various mechanisms, which can facilitate or inhibit DNA-templated activities.[1,5]

Several remodelers have been shown to impact protein-coding mRNA expression.[1,2] In murine embryonic stem (ES) cells, esBAF, NuRD, and Tip60-p400 have been characterized as major regulators of mRNA expression that cooperate with and antagonize one another to maintain the pluripotent state of the cell.[6–8] Additional remodelers, including SNF2H, INO80, CHD1, CHD2, CHD8, and SMARCAD1, play smaller yet still important roles in mRNA regulation in ES cells that contribute to pluripotency and other processes.[9–17] However, the contributions of most remodelers to non-protein-coding RNA expression, including major transcriptional regulators such as the NuRD and Tip60-p400 complexes, remain unexplored.

Non-protein-coding transcription gives rise to non-coding RNAs (ncRNAs): diverse RNA species, some having well-established roles in regulating transcription and/or translation.[18] Examples of functional ncRNAs include ribosomal RNAs (rRNAs), transfer RNAs (tRNAs), and microRNAs (miRNAs), among others. The functions of non-coding transcription originating from *cis*-regulatory elements (CREs), including promoters (upstream antisense RNAs [uaRNAs]) and enhancers (enhancer RNAs [eRNAs]), remain less well defined.[18] Cells must activate networks of enhancers and promoters to drive appropriate mRNA expression in response to signaling cues; in parallel, active enhancers and promoters produce eRNAs and uaRNAs, respectively. Initially proposed as non-functional byproducts of active CREs,[18–21] several studies implicate uaRNAs and eRNAs in *cis* mechanisms of transcriptional regulation, including RNA polymerase II promoter-proximal pausing,[22–24] recruitment of factors responsible for enhancer-promoter looping,[25] prolonged occupancy of transcription factors (TFs) at CREs,[26–28] and uaRNA- or eRNA-dependent deposition of histone modifications.[29,30] Chromatin-associated RNA mapping has found that eRNAs associate with target promoters in *trans* to drive gene activation.[27,30,31] Recently, eRNA-uaRNA duplex formation through complementary ALU elements was shown to contribute to enhancer-promoter looping and, therefore, mRNA regulation.[32] Collectively, this body of work demonstrates critical functional roles for CRE-associated ncRNAs and, therefore, necessitates novel lines of inquiry into the regulators of uaRNA and eRNA expression.

Many remodelers bind enhancers and promoters to regulate gene expression[9,15,33–45]; however, only a handful have been

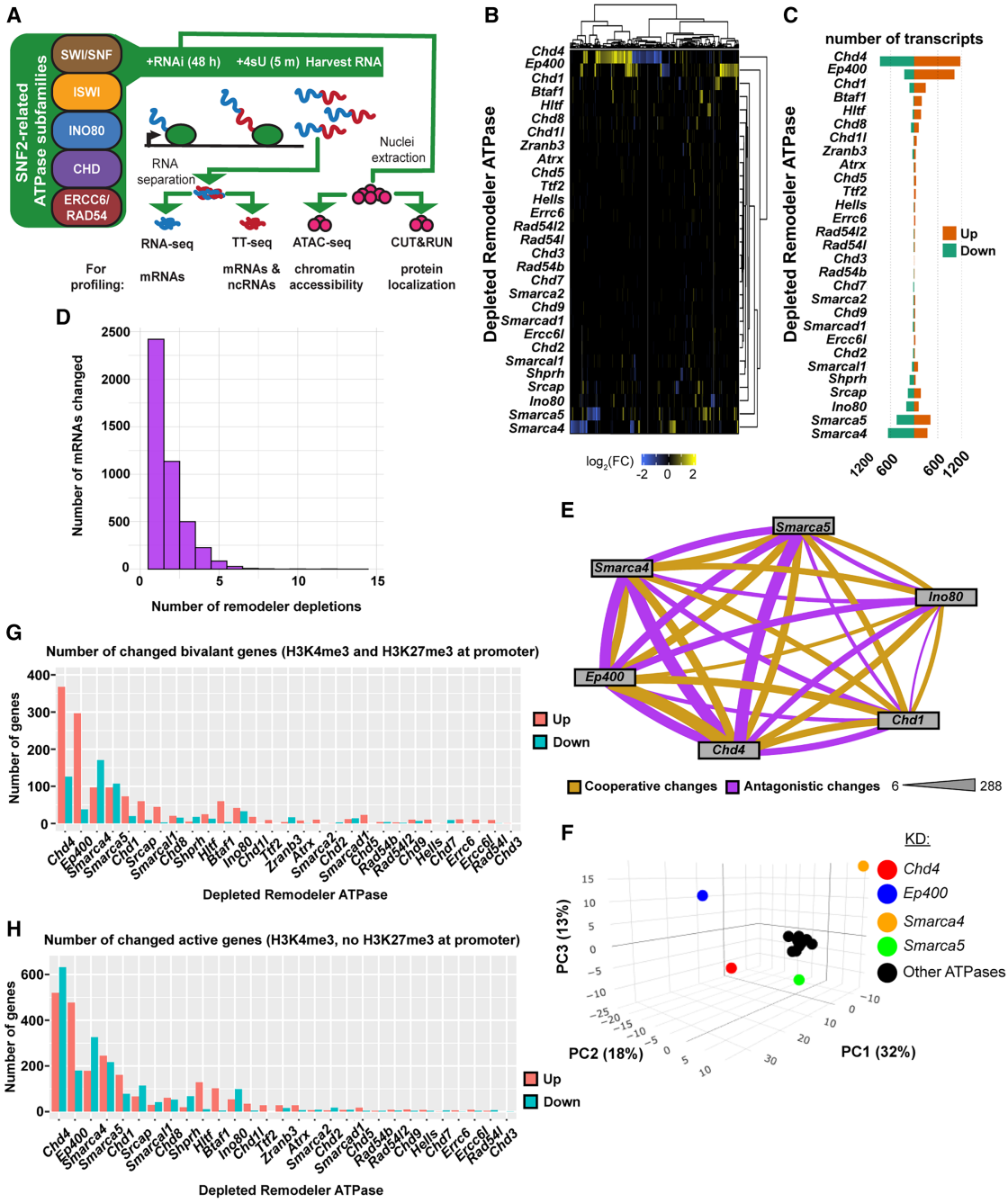

Figure 1. Remodeler ATPases collectively regulate thousands of mRNAs

(A) Experimental design for this study. 32 SNF2-related ATPases representing five families were targeted via RNAi in murine ES cells, and the transcriptomic consequences of individual depletions were examined using nascent (TT-seq) and steady-state (RNA-seq) approaches. Three ATPases were further examined using genome-wide chromatin accessibility (ATAC-seq) and protein localization (CUT&RUN) profiling.

(B) Heatmap showing the change in mRNA transcription for genes changed across all TT-seq datasets ($|\log_2$ fold change $[\log_2(FC)]| \geq 0.75$ and false discovery rate [FDR] ≤ 0.05). $n = 4{,}418$ transcripts.

(C) Barplot quantifying the number of mRNAs with increased (orange) or decreased (green) transcription upon remodeler depletion using TT-seq ($|\log_2(FC)| \geq 0.75$ and FDR ≤ 0.05).

(D) Histogram showing the distribution of mRNAs with altered transcription in one or more depletion datasets using TT-seq ($|\log_2(FC)| \geq 0.75$ and FDR ≤ 0.05).

(E) Network representing the number of mRNAs with altered transcription in the same direction (cooperative, gold) or opposite direction (antagonistic, purple) shared between six depletion TT-seq datasets ($|\log_2(FC)| \geq 0.75$ and FDR ≤ 0.05). Thickness of line represents the number of mRNAs shared between datasets within the range listed.

(legend continued on next page)

shown to play a direct role in ncRNA production at CREs.[46–48] esBAF suppresses the production of eRNAs and uaRNAs at target CREs by maintaining the positioning of adjacent nucleosomes.[48] INO80 and BTAF1 directly suppress uaRNA transcription in ES cells,[46] while CHD8 activity at progesterone receptor-dependent enhancers is necessary for eRNA expression.[47] Given the broad diversity of remodelers that localize to CREs in metazoan systems and the potential mechanisms by which they modulate chromatin dynamics, we systematically assessed how each remodeler contributes to the regulation of the ES cell transcriptome. To that end, we screened SNF2-type nucleosome remodelers for mRNA, uaRNA, and eRNA regulatory roles using RNA interference (RNAi) followed by paired steady-state and nascent transcriptome profiling to define the contributions of every remodeler to coding and non-coding transcription. We found that many remodelers regulate thousands of mRNAs, uaRNAs, and eRNAs. Our analyses support previous work showing coordinated regulation between mRNA and eRNA, but not mRNA and uaRNA, transcription. Finally, chromatin-based mechanistic studies suggest two classes of transcription regulation by remodelers: direct regulation through classical mechanisms such as TF interactions and indirect regulation through the maintenance of genomic stability.

RESULTS

Screen to define the nucleosome remodeler-regulated ES cell transcriptome

To systematically determine how nucleosome remodelers regulate the transcriptome, we performed an RNAi screen, individually targeting the 32 SNF2-like remodelers in ES cells (Figure 1A). We depleted the SNF2-like ATPase and quantified changes in the coding and non-coding transcriptomes using RNA sequencing (RNA-seq) and transient transcriptome sequencing (TT-seq[49]) from the same samples in biological duplicate or triplicate with high reproducibility (Figure S1A). We validated the depletion of 29 remodeler ATPases using RT-qPCR, RNA-seq, and, for a subset, western blotting (Figure S1B; Table S1). For three ATPases, *Chd6*, *Smarca1*, and *Ercc6l2*, we could not obtain depletion of 50% or better (as quantified by RT-qPCR and RNA-seq) and, therefore, did not proceed further with these candidates.

Nucleosome remodelers drive the appropriate transcription of thousands of mRNAs

To understand how remodelers impact the ES cell mRNA transcriptome, we analyzed genome-wide mRNA abundance (RNA-seq) and transcription (pre-mRNA levels; TT-seq) following individual remodeler depletion. We focused on 21,596 protein-coding genes from Gencode,[50] with 15,307 sufficiently transcribed for differential analysis (Figure S2A). Across datasets, we defined 5,810 differentially expressed mRNAs (RNA-seq) and 4,418 differentially transcribed mRNAs (TT-seq; Figures 1B, 1C, S2B, and S2C). RNA-seq and TT-seq profiles were similar in most remodeler depletions, exemplified by *Chd4* and *Smarca4* depletion (Figures S2D and S2E).

The largest number of mRNA changes occurred upon depletion of *Chd4*, *Smarca4*, or *Ep400*, encoding the ATPases of NuRD (CHD4), esBAF (BRG1), and Tip60-p400 (p400) complexes.[6–8,51] Fewer changes were observed for *Smarcad1*, *Smarca5*, *Ino80*, *Srcap*, *Chd1*, *Btaf1*, or *Chd8*, all previously implicated in mRNA regulation, and for ATPases less defined in transcription (*Hltf*, *Zranb3*, *Shprh*, and *Smarcal1*; Figures 1B, 1C, S2B, and S2C).[46,52–55] Depletion of other remodelers caused minimal transcriptomic changes, with the exception of *Ttf2* and *Chd7*. As expected, rapid 3-h depletion of CHD4, CHD8, and HLTF via dTAG yielded fewer transcriptional changes compared to 48-h knockdown (KD) (Figures S2F–S2O).

We examined how each remodeler depletion altered the expression of the other 31 SNF2-like ATPases. Most depletions had no effect, but ten ATPase depletions significantly changed the mRNA levels of other remodelers, with *Ttf2* and *Chd7* altering many, and *Smarca4*, *Hltf*, *Chd4*, *Chd8*, *Smarca5*, *Ino80*, *Srcap*, or *Ep400* affecting a smaller subset (Figure S2P).

When assessing mRNA specificity, 55% of differentially transcribed mRNAs were altered by only one remodeler depletion, whereas 45% were affected by two or more, consistent with previous reports that remodeler binding at CREs shows substantial overlap (Figure 1D; Table S2).[44] To better understand overlapping regulation of mRNA transcription by remodelers, we examined the shared (cooperative) or opposite (antagonistic) effects on mRNA transcription between p400, BRG1, CHD4, SNF2H, CHD1, and INO80, all of which are remodelers with established roles in pluripotency regulation (Figure 1E).[6–9,11,15] *Smarca4* and *Chd4* KD displayed the largest number of mRNAs with antagonistic changes, in line with prior studies,[56,57] whereas *Chd4* and *Ep400* had the most overlapping mRNAs with cooperative changes. Toward understanding the regulatory relationships between all remodelers, we examined differential transcription across all datasets using principal-component analysis (PCA) on 851 mRNAs changed in 3 or more remodeler depletions and found that CHD4, p400, BRG1, and SNF2H primarily drive overlapping mRNA regulation (Figure 1F). Overall, these data confirm CHD4, p400, BRG1, and SNF2H as the major drivers of mRNA regulation among remodelers in ES cells but highlight the contribution of all remodelers in regulating mRNA expression.

Epigenomic analyses reveals roles for BTAF1, CHD8, SRCAP, SMARCAL1, SHPRH, and HLTF in regulating transcription of bivalent and/or active genes

To assess whether local epigenomic environments categorize mRNA regulation by remodelers, we analyzed chromatin immunoprecipitation (ChIP)-seq datasets from wild-type (WT) ES cells[58] to define promoters enriched for H3K4me3 (active genes) or both H3K4me3 and H3K27me3 (bivalent genes).[59,60] Depletion of *Smarca4*, *Ep400*, *Chd4*, *Chd1*, or *Smarca5* altered the

(F) PCA plot of differential transcription data from TT-seq where mRNAs changed in 3 or more depletions. $n = 892$ transcripts.
(G) Barplot showing the numbers of mRNAs with increased (orange) or decreased (green) transcription from TT-seq data ($|\log_2(FC)| \geq 0.75$ and FDR ≤ 0.05) for promoters displaying bivalent chromatin signatures (H3K4me3 and H3K27me3).
(H) As in (G) but for promoters displaying active chromatin signatures (H3K4me3 and no H3K27me3).

transcription of bivalent genes (Figure 1G), consistent with known roles in pluripotency.[6,7,15,44,61] These findings demonstrate the utility of integrating transcriptomic and epigenomic data and prompted the exploration of less-studied remodelers.

Therefore, we next examined H3K4me3 and H3K27me3 profiles for genes altered in each remodeler depletion. Similar to *Chd4* and *Ep400*, *Srcap* and *Smarcal1* depletion led to the upregulation of bivalent genes (Figure 1G), suggesting roles in pluripotency. In contrast, *Chd8* depletion primarily affected the transcription of H3K4me3-marked genes, consistent with previous findings showing limited CHD8 and H3K27me3 overlap (Figures 1G and 1H).[44] Similarly, *Shprh* and *Hltf* depletion altered the transcription of H3K4me3-marked genes. *Btaf1* depletion upregulated both bivalent and active genes, supporting a broad role in transcription regulation.[46] Overall, these integrated analyses confirm established trends (CHD4 and p400), reinforce proposed roles (BTAF1, SRCAP, and CHD8), and suggest undescribed functions for SMARCAL1, HLTF, and SHPRH.

Remodeler depletions disrupt non-coding transcription at thousands of promoters

Divergent transcription from mRNA promoters produces ncRNAs termed uaRNAs (also promoter-associated ncRNAs [pancRNAs] or promoter upstream transcripts [PROMPTs]).[62,63] Prior studies showed that BRG1, INO80, and BTAF1 suppress non-coding transcription in ES cells,[46,48] with BAF, CHD1, and SNF2H yeast homologs regulating non-coding transcription within gene bodies.[64–66] Using our TT-seq datasets, we defined the remodeler-dependent uaRNA transcriptome. We detected antisense transcription from 4,856 promoters, with 2,692 showing significantly altered uaRNA transcription across depletions, representing highly transcribed eRNAs (Figures 2A, 2B, S3A, and S3B). Remodelers altering the most mRNAs also affected the most uaRNAs (Figure S3C).

Depletion of *Smarca4*, *Hltf*, *Btaf1*, *Chd1*, or *Smarca5* mainly upregulated uaRNAs (repressors), while depletion of *Chd4*, *Chd8*, or *Smarcal1* mainly downregulated uaRNAs (activators); other remodelers (e.g., *Ep400*, *Ino80*, *Shprh*, *Chd2*, or *Zranb3*) showed both up- and downregulation of uaRNAs (Figures 2A and 2B; Table S2). These remodeler ATPases or their orthologs localize to promoter elements in metazoan systems,[35,44,45,54,67] suggesting possible direct regulation of uaRNA transcription. When evaluating the specificity of remodelers in uaRNA regulation, we found that only 24% of altered uaRNAs were unique to one remodeler depletion (Figure 2C; Table S2), indicating more overlapping changes by remodelers compared to mRNAs (55%; Figure 1D; Table S2).

To explore remodeler relationships, we analyzed cooperative and antagonistic effects on uaRNAs among repressors (BRG1, HLTF, and BTAF1) and activators (CHD4, SMARCAL1, and CHD8; Figure 2D). Repressors and activators showed cooperation within classes and antagonism between classes. PCA of 1,307 uaRNAs changed in 3 or more remodeler depletions revealed that PC1 was defined by *Chd4* KD antagonism with repressors and cooperation with activators; PC2 by the distinction of p400 from all other remodelers, most likely due to its strong bidirectional effect on uaRNA transcription; and PC3 by *Smarca4*, *Smarca5*, and other repressors (Figure S3D). These analyses show, as with mRNA regulation, that BRG1, p400, CHD4, and SNF2H strongly regulate uaRNA transcription and identify remodelers as repressors, activators, or bidirectional regulators of uaRNA transcription.

Nucleosome remodelers independently regulate uaRNA and mRNA transcription at shared promoters

Prior studies demonstrate that levels of mRNA and uaRNA transcription from a shared promoter generally correlate,[19,20,68] suggesting that the regulatory effects of remodelers would impact both transcripts originating from a shared promoter. We hypothesized that changes in uaRNA and mRNA transcription would be correlated upon remodeler depletion, given that the transcripts share a common promoter. To our surprise, we found minimal coordination between mRNA and uaRNA transcription across all remodeler depletions (Figure 3). Two examples are *Smarca4* KD and *Smarcal1* KD (Figures 3A and 3B), where only 66 of 1,994 promoters (*Smarca4* KD) and 1 of 412 promoters (*Smarcal1* KD) showed concordant changes in both mRNA and uaRNA transcription.

To assess the coordination of uaRNA and mRNA transcription regulation by all remodelers, we sorted uaRNA-producing promoter elements into six categories based on mRNA and uaRNA change (mRNA only up, mRNA only down, uaRNA only up, uaRNA only down, same directional change, and opposite directional change). We found that for most promoters, remodeler depletion specifically affected only mRNA or uaRNA transcription, with concordant or discordant directional changes comprising less than 5% of all affected promoters (Figure 3C). Consistent with this, the same directional change and opposite directional change categories were rarely represented in any remodeler depletion and were never statistically enriched (Figure S3E). When comparing promoter directionality in these categories for each remodeler depletion relative to control, we found shifts in directionality consistent with changes in one transcript but not the other (exemplified with *Smarca4* KD and *Smarca5* KD; Figures S3F and S3G). These data demonstrate that the impact of remodeler depletion on mRNA or uaRNA regulation is not coordinated, further suggesting that mRNA and uaRNA transcription is not co-regulated by remodelers.

Two potential explanations for these findings are that promoters showing only mRNA change do not express uaRNAs or that these uaRNAs are not detectable by TT-seq. To evaluate these possibilities, we quantified uaRNA transcription from promoters showing only mRNA or uaRNA changes for a subset of 12 remodelers with at least 50 changed promoters in each group. We found that non-coding transcription could be measured at promoters showing only mRNA change (Figures S3H and S3I). While it remains unclear whether our findings extend to promoters with low or undetectable uaRNA transcription, these data support the idea that the effects of remodeler depletion on mRNA and uaRNA transcription are largely independent.

Widespread impact of remodelers on eRNA transcription

Another major class of CRE-associated ncRNAs is eRNAs. To assess remodeler influence on non-coding transcription from

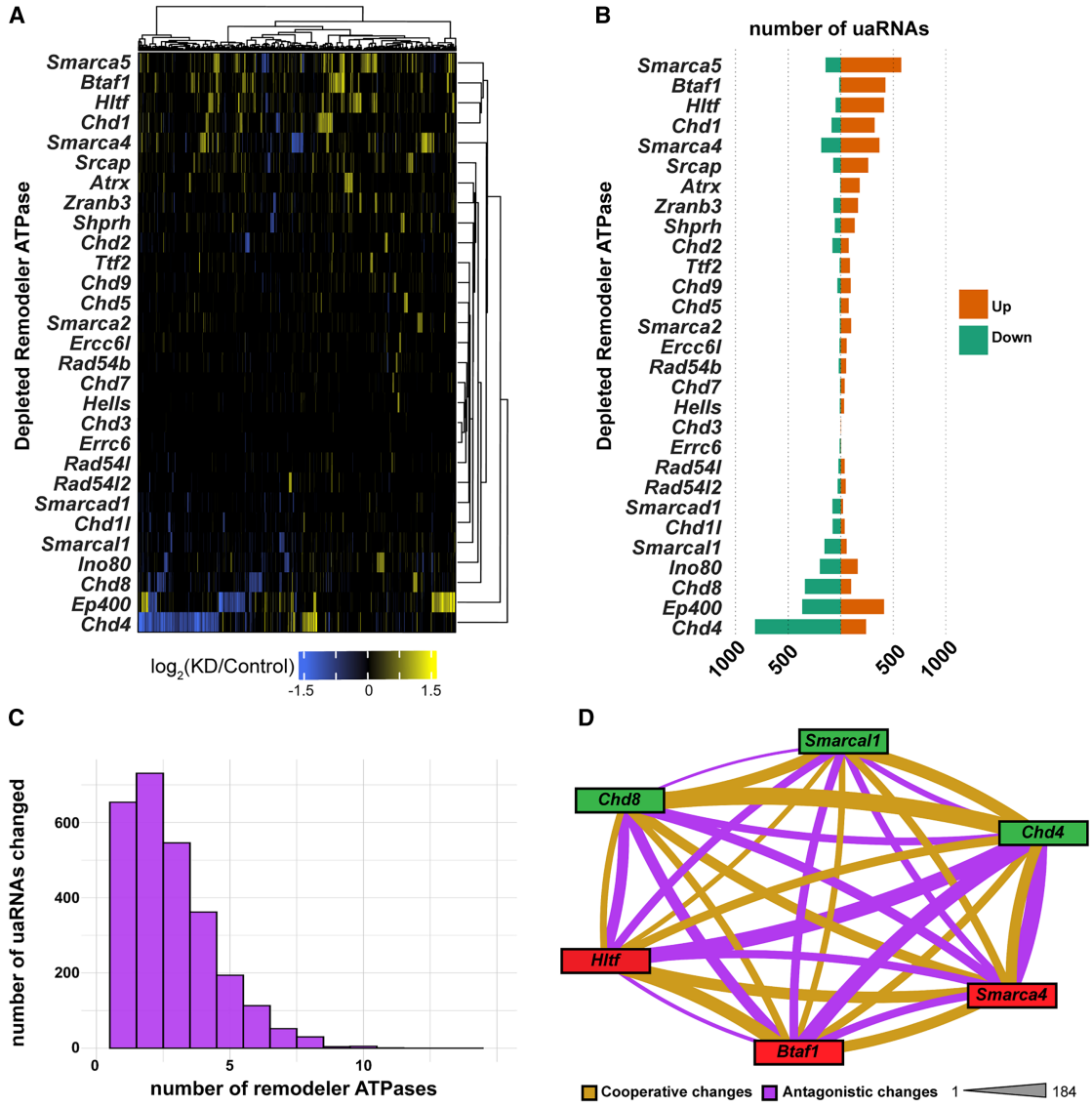

Figure 2. Many remodelers contribute to uaRNA transcription regulation in ES cells

(A) Heatmap showing the change in transcription of uaRNAs for transcripts changed across all TT-seq datasets ($|\log_2(FC)| \geq 0.5$ and FDR ≤ 0.05). n = 2,692 transcripts.

(B) Barplot quantifying the number of uaRNAs with increased (orange) or decreased (green) transcription in each depletion TT-seq dataset ($|\log2(FC)| \geq 0.5$ and FDR ≤ 0.05).

(C) Histogram showing distribution of uaRNAs altered in one or more depletion TT-seq dataset(s) ($|\log_2(FC)| \geq 0.5$ and FDR ≤ 0.05).

(D) Network representing the number of uaRNAs with altered transcription in the same direction (cooperative, gold) or opposite direction (antagonistic, purple) shared between six depletion datasets ($|\log_2(FC)| \geq 0.5$ and FDR ≤ 0.05). Thickness of line represents the number of uaRNAs in the category shared between datasets within the range listed. Green labels indicate "activator" class and red indicate "repressors" class remodelers.

enhancer elements in ES cells, we annotated 101,587 putative enhancers from TSS-distal DNase I hypersensitive sites (DHSs[69]). TT-seq detected transcription from 22,016 TSS-distal DHSs (Figure S4A), consistent with other studies,[70–72] which we define as putative enhancers/eRNAs. Across all depletions, 10,039 putative eRNAs (46%) exhibited altered transcription in at least one remodeler depletion (Figures 4A, 4B, and S4A), representing highly transcribed eRNAs (Figure S4B).

Consistent with our mRNA and uaRNA findings, *Chd4*, *Ep400*, *Smarca5*, and *Smarca4* depletion led to the largest numbers of altered putative eRNAs (Figures 4A and 4B; Table S2). Depletion of other remodelers important for eRNA transcription in ES cells or other systems, including *Ino80*, *Chd8*, and *Chd1*, also robustly altered the transcription of putative eRNAs.[38,47,76] Beyond these previously characterized regulators, we observed changes in putative eRNA transcription in every remodeler depletion, with one

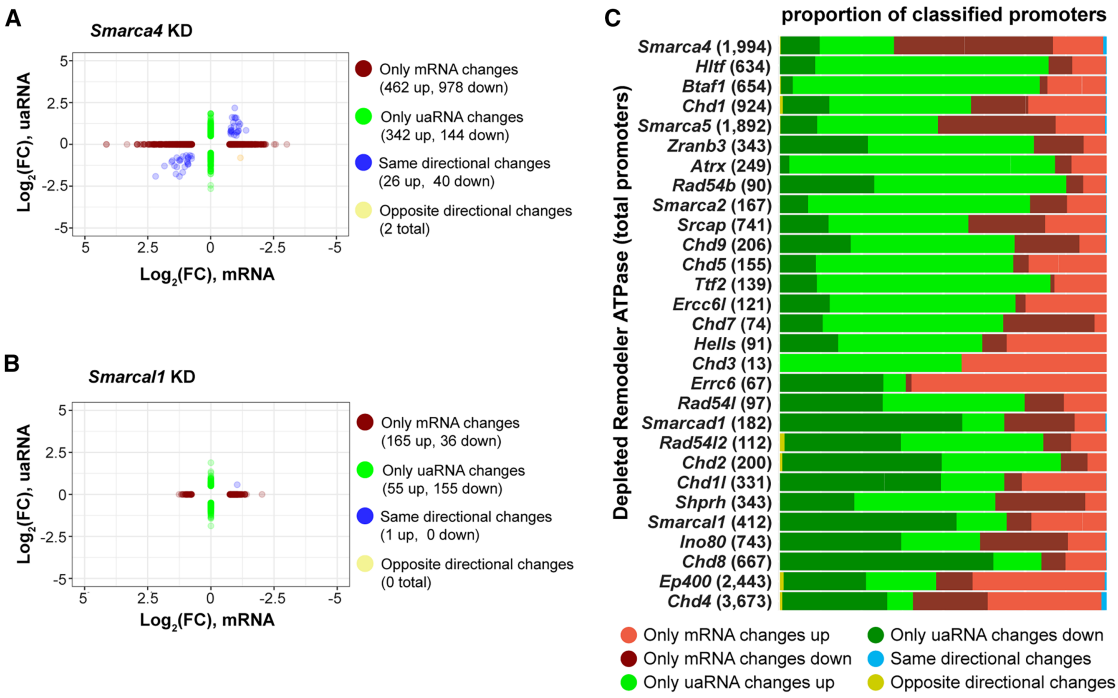

Figure 3. Changes in mRNA and uaRNA transcription with a shared promoter are not coordinated

(A) Scatterplot showing changes in mRNA versus uaRNA transcription in *Smarca4* depletion from TT-seq data. Colors represent promoters sorted into four categories based on mRNA and/or uaRNA change: red, promoters with only significant mRNA changes (mRNA change $|\log_2(FC)| \geq 0.75$ and FDR ≤ 0.05, no significant change in uaRNA transcription); green, promoters with only significant uaRNA changes (uaRNA change $|\log_2(FC)| \geq 0.5$ and FDR ≤ 0.05, no significant change in mRNA transcription); blue, promoters with significant changes in both transcripts in the same direction (mRNA change $|\log_2(FC)| \geq 0.75$ and FDR ≤ 0.05 and uaRNA change $|\log_2(FC)| \geq 0.5$ and FDR ≤ 0.05, in the same direction); and yellow, promoters with significant changes in both transcripts in opposing direction (mRNA change $|\log_2(FC)| \geq 0.75$ and FDR ≤ 0.05 and uaRNA change $|\log_2(FC)| \geq 0.5$ and FDR ≤ 0.05, in the opposing direction).

(B) Same as in (A) but for *Smarcal1* depletion.

(C) Barplot displaying the relative distribution of promoters with significant mRNA or uaRNA changed in TT-seq datasets sorted into six categories based on the directional change of each transcript. mRNA change: $|\log_2(FC)| \geq 0.75$ and FDR ≤ 0.05 and uaRNA change: $|\log_2(FC)| \geq 0.5$ and FDR ≤ 0.05. Numbers in parentheses indicate the total number of promoters showing significant change in mRNA and/or uaRNA change.

remodeler depletion changing the transcription of over 1,000 putative eRNAs (*Hltf* KD), and the remaining altering the transcription of fewer putative eRNAs (Figures 4A and 4B; Table S3). Further, the number of putative eRNAs changed was proportional to the number of mRNAs changed upon each remodeler depletion (Figure S4C). Notably, 75% of changed eRNAs were altered in two or more depletions (Figure S4D). Our data reveal widespread remodeler impact on eRNA transcription in ES cells.

We next analyzed pairwise regulatory interactions among the six remodeler depletions with the largest effects on eRNA transcription (*Chd4*, *Ep400*, *Smarca4*, *Smarca5*, *Hltf*, and *Smarcal1*). *Smarcal1* showed balanced cooperative/antagonistic relationships with *Smarca4*, *Chd4*, and *Smarca5* but stronger antagonism with *Ep400* (Figure S4E). *Hltf* exhibited balanced relationships with *Smarca4*, *Chd4*, and *Ep400* but cooperated strongly with *Smarca5*. These data show specificity in the regulatory interactions with two understudied remodelers and previously established regulators of transcription in ES cells. We further probed the regulatory interactions among all remodelers through PCA using differential transcription data focused on putative eRNAs changed in 3 or more remodeler depletions ($n = 5,143$ putative eRNAs; Figure S4F). PC1–3 were shaped by *Chd4*, *Ep400*, *Smarca4*, and *Smarca5* interactions (Figure S4F), similar to the mRNA data. Overall, our data demonstrate broad eRNA regulation by remodelers, with major contributions from CHD4, p400, BRG1, and SNF2H, and identify SMARCAL1 and HLTF as regulators of eRNA transcription.

Remodeler depletions induce coordinated changes in putative eRNA and mRNA transcription

Current models suggest that changes in transcription from functionally associated enhancers and mRNAs correlate with one another,[77] leading us to hypothesize that putative enhancer-promoter pairs (EPPs) would show correlated changes within our remodeler depletion TT-seq datasets. We performed an *in silico* search for EPPs showing correlated transcription change within our TT-seq data across multiple distance thresholds (100 kb, 250 kb, 500 kb, and 1 Mb; see STAR Methods). Consistent with our hypothesis, we detected significantly more putative EPPs than expected by chance across 3 or more distance thresholds for 16 remodeler depletions (Figures S5A and S5B). The median distance between EPPs within each depletion at the 500 kb threshold ranged from 96 to 225 kb (Figure S5C), well within the range of functionally validated EPPs in mammalian systems.[78,79]

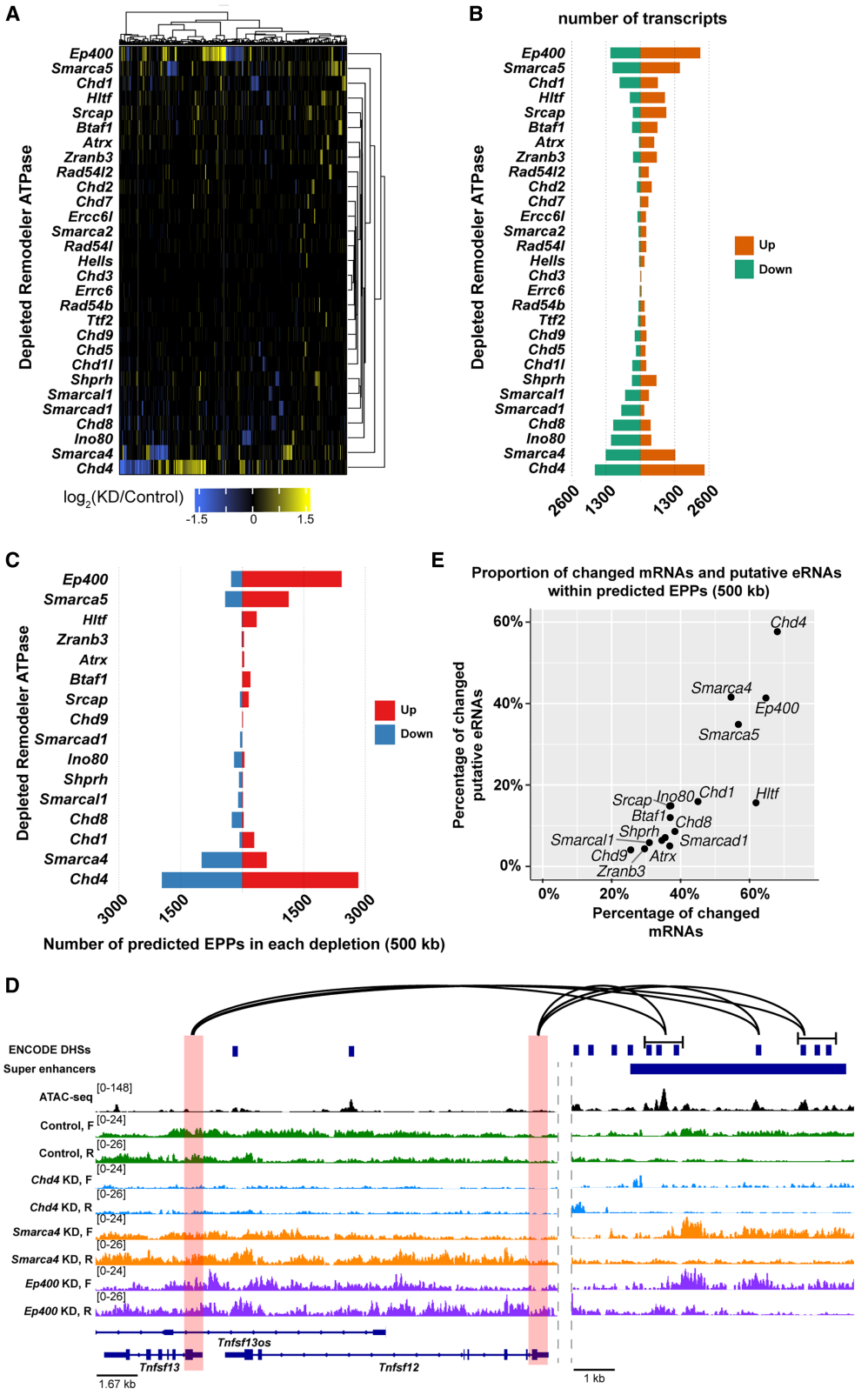

(legend on next page)

Included in remodeler depletions that displayed significant enrichment for EPPs were known or suspected regulators of enhancer activity, CHD4, BRG1, SNF2H, p400, CHD1, INO80, and CHD8. Several other remodelers behaved similarly to (or had a greater enrichment than) these known enhancer regulators, including HLTF, SHPRH, SMARCAL1, BTAF1, SRCAP, SMARCAD1, and ATRX (Figures S5A and S5B). These analyses suggest that depletion of at least 16 remodelers induces coordinated mRNA and putative eRNA transcriptional changes. We selected the 500 kb distance threshold for further characterization.

Chd4, *Ep400*, *Smarca5*, and *Smarca4* depletions displayed the largest numbers of changed EPPs (Figure 4C). Based on our analysis of published promoter capture Hi-C data,[73–75] we found that predicted EPPs included correlated transcription changes between super-enhancers and target genes, supporting our identification of functional interactions (Figures 4D and S5D). We found that 23%–69% of changed mRNAs and 10%–60% of putative eRNAs could be assigned to EPPs across these 16 depletions (Figure 4E). Gene Ontology (GO) analyses of changed mRNAs in upregulated and downregulated EPPs in each of the 16 depletions are consistent with known functions for these remodelers (Figures S5E and S5F). These analyses suggest coordinated changes in putative eRNA and mRNA transcription following the depletion of at least 16 remodelers.

CHD8 and SRCAP, but not SMARCAL1, co-localize with transcriptomic changes

We selected three ATPases for further studies, CHD8, SRCAP, and SMARCAL1, to mechanistically determine how these remodelers act to regulate the ES cell transcriptome. First, we examined the chromatin localization of these three remodelers using cleavage under target and release using nuclease (CUT&RUN) for SRCAP and SMARCAL1 after testing three antibodies for each remodeler and by analyzing available ChIP-seq data from ES cells for CHD8.[44] We defined 30,053, 50,743, and 2,271 peaks for CHD8, SRCAP, and SMARCAL1, respectively (Figures S6A–S6C). To examine whether these factors may be acting directly at locations of transcription changes, we integrated our transcriptomic and localization data for each remodeler. We found that CHD8 and SRCAP bound many of the promoters and enhancers with transcription changes upon depletion of these remodelers (Figures 5A and 5B). We observed minimal SMARCAL1 enrichment at changed CREs, suggesting indirect effects of SMARCAL1 loss on transcription (Figure 5C). These data suggest that CHD8 and SRCAP act directly to regulate transcription, while SMARCAL1 may act through indirect mechanisms.

Depletion of *Chd8*, *Srcap*, or *Smarcal1* results in limited changes to chromatin accessibility and H3K27ac enrichment

To investigate whether a chromatin-based mechanism explains the transcriptomic changes observed upon depletion of CHD8, SRCAP, or SMARCAL1, we analyzed chromatin accessibility by assay for transposon-accessible chromatin sequencing (ATAC-seq) and H3K27ac enrichment by CUT&RUN following the depletion of *Chd8*, *Srcap*, or *Smarcal1*. Depletion of *Chd8*, *Srcap*, or *Smarcal1* abolished the enrichment of each remodeler on chromatin as determined by CUT&RUN and salt fractionation experiments (Figures S6D–S6I). Using ATAC-seq, we identified only 376, 686, and 315 regions with differential accessibility upon depletion of *Chd8*, *Srcap*, and *Smarcal1*, respectively, with minimal overlap of CREs with changes in transcription (Figure S6J). We detected 21, 321, and 211 differentially enriched H3K27ac regions upon the depletion of *Chd8*, *Srcap*, and *Smarcal1*, respectively, with little overlap with changes in transcription (Figure S6K). These data suggest that CHD8, SRCAP, and SMARCAL1 work through alternative mechanisms to regulate transcription.

CHD8 functionally interacts with NFY, ETS, and p53 family TFs to regulate transcription

To test whether the depletion of *Chd8*, *Srcap*, or *Smarcal1* may influence TF binding, we integrated ATPase localization and ATAC-seq data upon remodeler depletion to analyze TF footprints at promoters and putative enhancers bound by these factors using TF occupancy prediction by investigation of ATAC-seq signal (TOBIAS).[80] TOBIAS compares accessibility over TF motifs to infer differences in TF binding between experimental conditions, providing a proxy for how TF binding profiles change between conditions. Upon *Chd8* depletion, we observed a strong and specific decrease in the predicted binding of ETS- and NFY-related factors and a moderate increase in the predicted binding of p53-related factors at both promoters and putative enhancers, with the strongest effect at CREs bound by CHD8 (Figures 5D and 5E). CHD8 has been reported as a positive regulator of ETS-family factor binding in human neurons[81] and a negative regulator of p53 binding in ES cells,[10,82,83] both validating our approach and suggesting a conserved role between CHD8 and ETS factors in ES cells. The association between NFY binding and CHD8 represents a previously unestablished regulatory interaction. Therefore, we assessed changes in

Figure 4. Coordinated regulation of mRNA and enhancer transcription in remodeler depletions

(A) Heatmap showing the change in transcription of putative enhancers ($|\log_2(FC)| \geq 0.5$ and FDR ≤ 0.05) across TT-seq datasets. n = 10,039 regions.

(B) Barplot showing the total number of putative enhancers with increased (orange) or decreased (green) transcription in each depletion TT-seq dataset ($|\log2(FC)| \geq 0.5$ and FDR ≤ 0.05).

(C) Barplot showing the number of predicted enhancer-promoter pairs (EPPs) with increased or decreased transcription in each TT-seq dataset based on a 500 kb distance threshold.

(D) Browser track showing chromatin accessibility (ATAC-seq) and comparing transcription (TT-seq) in the control, *Chd4* KD, *Smarca4* KD, and *Ep400* KD over the *Tnfsf12* locus and the interacting super-enhancer region. Red boxes highlight promoter regions of each locus, and lines indicate DHSs within the super-enhancer region shown to interact with each promoter as shown using available promoter capture HiC data.[73–75]

(E) Scatterplot showing the relative proportions of significantly changed mRNAs and putative eRNAs that could be placed into predicted EPPs in each depletion dataset based on a 500 kb distance threshold.

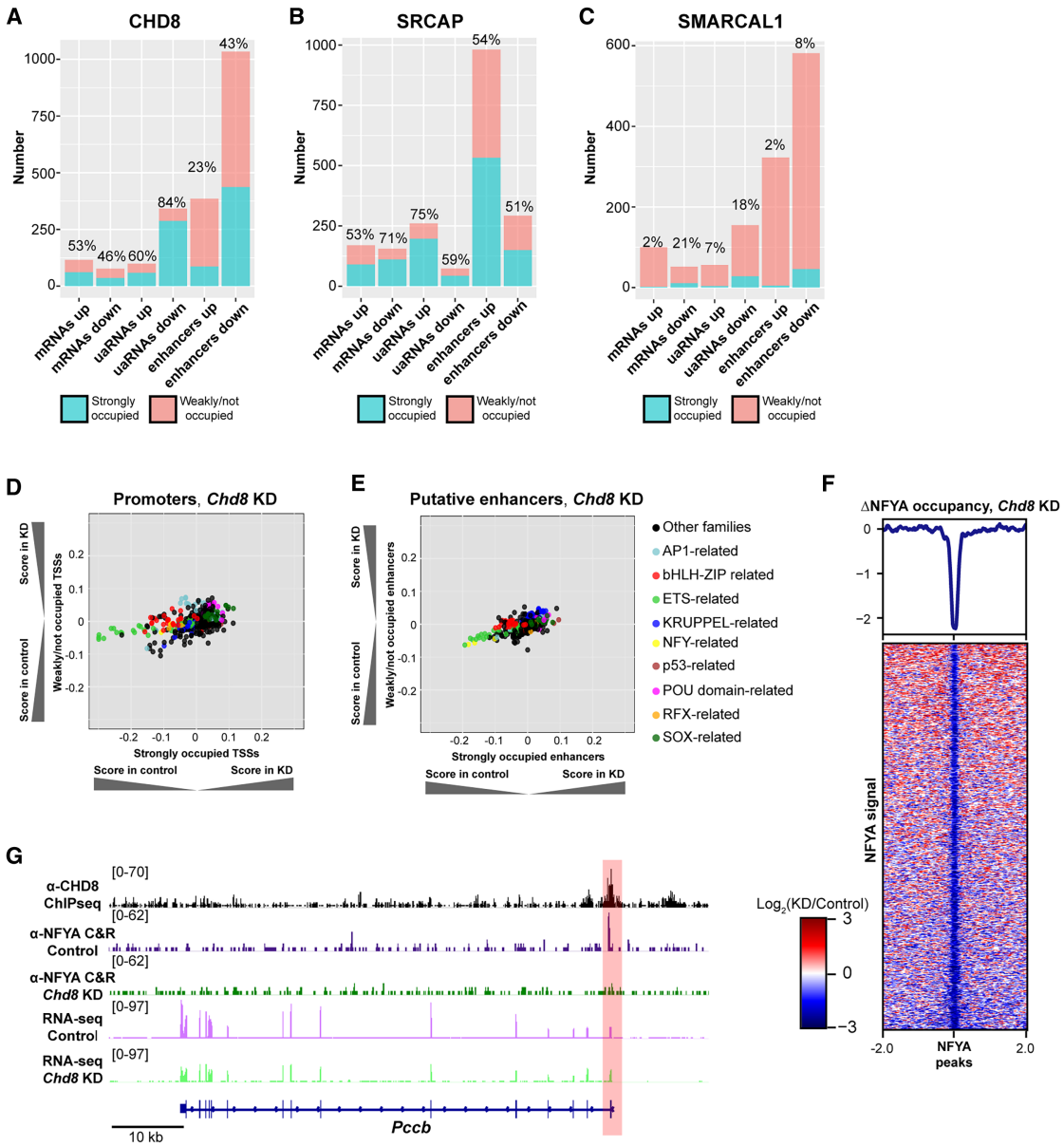

Figure 5. CHD8 functionally interacts with NFY, ETS, and p53 family transcription factors to regulate transcription

(A) Barplot showing the number of CREs within each altered transcript class bound by CHD8 using available ChIP-seq data (GEO: GSE64825; see also De Dieuleveult et al.[44]). Blue represents number of strongly bound elements, and pink indicates number of weakly bound or unbound elements.

(B) As in (A) but for SRCAP binding using CUT&RUN.

(C) As in (A) but for SMARCAL1 binding using CUT&RUN.

(D) Scatterplot comparing the binding score of different TF motifs at promoters bound versus not bound by CHD8. Motifs representing factors from similar related groups are colored according to the legend. All factors shown have $p \leq 0.05$ at bound and unbound loci, defined from ATAC-seq data using TOBIAS.[80]

(E) As in (D) but for putative enhancers bound and unbound by CHD8.

(F) Heatmap showing differential NFYA binding at all NFYA peaks in the *Chd8* KD relative to control CUT&RUN experiments. n = 1,179 peaks.

(G) Browser track showing chromatin accessibility (ATAC-seq) and comparing NFYA binding (CUT&RUN) and gene expression (RNA-seq) in the control and *Chd8* KD at the *Pccb* locus. Red box indicates the promoter region.

NFYA localization in *Chd8*-depleted ES cells relative to control using CUT&RUN. We observed a decrease in NFYA binding in *Chd8*-depleted ES cells, validating our findings from TOBIAS (Figure 5F). Changes in NFYA binding at promoters bound by CHD8 were associated with transcriptional changes, as exemplified by *Pccb* (Figure 5G). In *Chd8*-depleted ES cells, we very stringently defined 33 gained and 96 lost NFYA peaks relative to control ES cells (Figure S7A). Using an available

ChromHMM map of the ES cell genome,[84] we found that lost peaks were significantly enriched for "active promoter" and "strong enhancer" chromatin states, while gained peaks were significantly enriched for active promoter, "intergenic," and "weak enhancer" states (Figures S7B and S7C). Notably, NFYA-, ETS-, or p53-family factors were not differentially expressed in *Chd8*-depleted ES cells (Table S1), supporting a regulatory interaction between CHD8 and these TFs rather than upstream transcriptional regulation by CHD8. In summary, we found that NFYA localization is dependent upon CHD8 in ES cells, and our analyses suggest that CHD8 regulates transcription through functional interactions with ETS-, p53-, and NFY-family TFs.

SRCAP drives expression of AP-1-related factors through appropriate H2A.Z localization

SRCAP and Tip60-p400 are the two remodelers known to incorporate histone variant H2A.Z into nucleosomes.[45,85,86] Upon depletion of *Srcap*, we found a specific increase in predicted binding of AP-1- and RFX-related family factors at promoters and putative enhancers (Figures 6A and 6B). Loss of H2A.Z localization is associated with increased binding of c-FOS (an AP-1 factor) at promoters in human epithelial cells[87] and increased FOS expression in mouse embryonic fibroblasts,[88] suggesting that SRCAP may also negatively regulate AP-1 TF binding in ES cells, perhaps through appropriate H2A.Z incorporation. To test this hypothesis, we determined H2A.Z localization in *Srcap*-depleted and control ES cells, finding that *Srcap* depletion results in decreased H2A.Z localization (Figure S7D), as expected given previously defined roles for SRCAP.[85] Differential peak analysis stringently identified 121 gained and 735 lost H2A.Z peaks in *Srcap*-depleted cells (Figures S7E–S7G). In line with our hypothesis, we observed reduced H2A.Z binding over FOSL2:JUN motifs in *Srcap*-depleted cells (Figure 6C). In support of direct transcriptional regulation of AP-1 TFs by SRCAP, AP-1-family TFs *Jun* and *Fosl2* were differentially expressed via RNA-seq in *Srcap*-depleted ES cells (Table S1). SRCAP binds the *Fosl2* promoter in WT cells, and, upon *Srcap* depletion, H2A.Z is lost, correlating with the increase in transcription observed (Figure 6D). Together, these data support a mechanism whereby SRCAP contributes to appropriate transcription of putative eRNAs and mRNAs through the incorporation of H2A.Z at specific loci, including AP-1 binding sites, and direct repression of AP-1 TF expression.

Regulatory interactions with the Integrator complex may explain changes in ncRNA transcription for remodelers associated with genomic stability

In contrast to CHD8 and SRCAP, TOBIAS analysis predicts minimal TF families with altered binding upon the depletion of SMARCAL1 (Figures S7H and S7I). In addition, given the small proportion of CREs bound by SMARCAL1 and the fact that none of the TOBIAS-identified factors are differentially expressed in *Smarcal1*-depleted cells, we did not pursue any candidate TFs.

In metazoans, post-transcriptional regulation of non-polyadenylated RNAs (including many eRNAs and uaRNAs) occurs at the level of transcription termination through the Integrator complex, which downregulates uaRNA and eRNA biogenesis through the cleavage of the nascent RNA and de-stabilization of RNA polymerase II.[89–92] Depletion of INTS11 (a component of the cleavage module of Integrator) is associated with a global change in eRNA and uaRNA transcription in ES cells.[93] We hypothesized that the altered binding of Integrator may explain changes in ncRNA transcription upon depletion for those remodelers where a direct chromatin- or TF-based mechanism was not obvious, such as for SMARCAL1. To test this hypothesis, we determined the localization of INTS5, a structural subunit of the Integrator complex, in *Smarcal1*-depleted and control ES cells using CUT&RUN. We detected an increase in INTS5 occupancy at promoters and putative enhancers in *Smarcal1*-depleted cells (Figures 7A and 7B).

Given these findings, we examined whether impaired Integrator function could be detected in remodeler depletions. In metazoans, Integrator is critical for proper transcription and 3′ end processing of replication-dependent histone genes and small nucleolar RNAs (snoRNAs).[89,90,94] To infer Integrator activity, we examined changes in nascent transcription of these gene sets in every remodeler depletion. Individual depletion of ten remodelers led to a strong upregulation of histone gene transcription, while the depletion of seven remodelers led to a downregulation of these mRNAs (Figures 7C and 7D), also reflecting enriched GO terms such as chromatin assembly or nucleosome organization for mRNAs in predicted EPPs in these depletions (Figures S5E and S5F). Notably, the depletion of several remodelers that were identified as uaRNA repressors in our screen (e.g., HLTF, BTAF1, and SNF2H; Figure 2) led to an upregulation of histone transcription, while the depletion of remodelers identified as uaRNA activators (e.g., CHD4, SMARCAL1, and SHPRH; Figure 2) led to a downregulation of histone gene transcription. Similar changes were observed for snoRNA transcription (Figures 7E and 7F). In summary, these results support a model wherein changes in Integrator recruitment, assembly, and/or function may contribute to the changes in ncRNA transcription detected at promoters and enhancers upon depletion of some nucleosome remodelers. We propose a model where remodelers act minimally through two broad classes: class 1 regulates coding and non-coding transcription through chromatin- and/or TF-based mechanisms and class 2, often remodelers with roles in genome stability, safeguards the genome through diverse activities that reinforce appropriate Integrator localization and ncRNA transcription (Figure 7G).

DISCUSSION

While a handful of the 32 SNF2-related remodelers have been defined as direct transcriptional regulators, many more have been proposed to fulfill this role. Leveraging the well-studied murine ES cell model, we systematically examined the transcriptional consequences of CREs upon individual depletion of 29 SNF2-related ATPases. Our findings support the regulatory paradigm that CHD4, BRG1, p400, and SNF2H act as key contributors to the mRNA transcriptome in ES cells, as demonstrated in previous studies,[6–8,11,43,44,95] with more modest, but still critical, contributions from CHD1, INO80, CHD8, SRCAP, and BTAF1[9,10,15,45,46,96] (Figure 1). Our study identifies additional

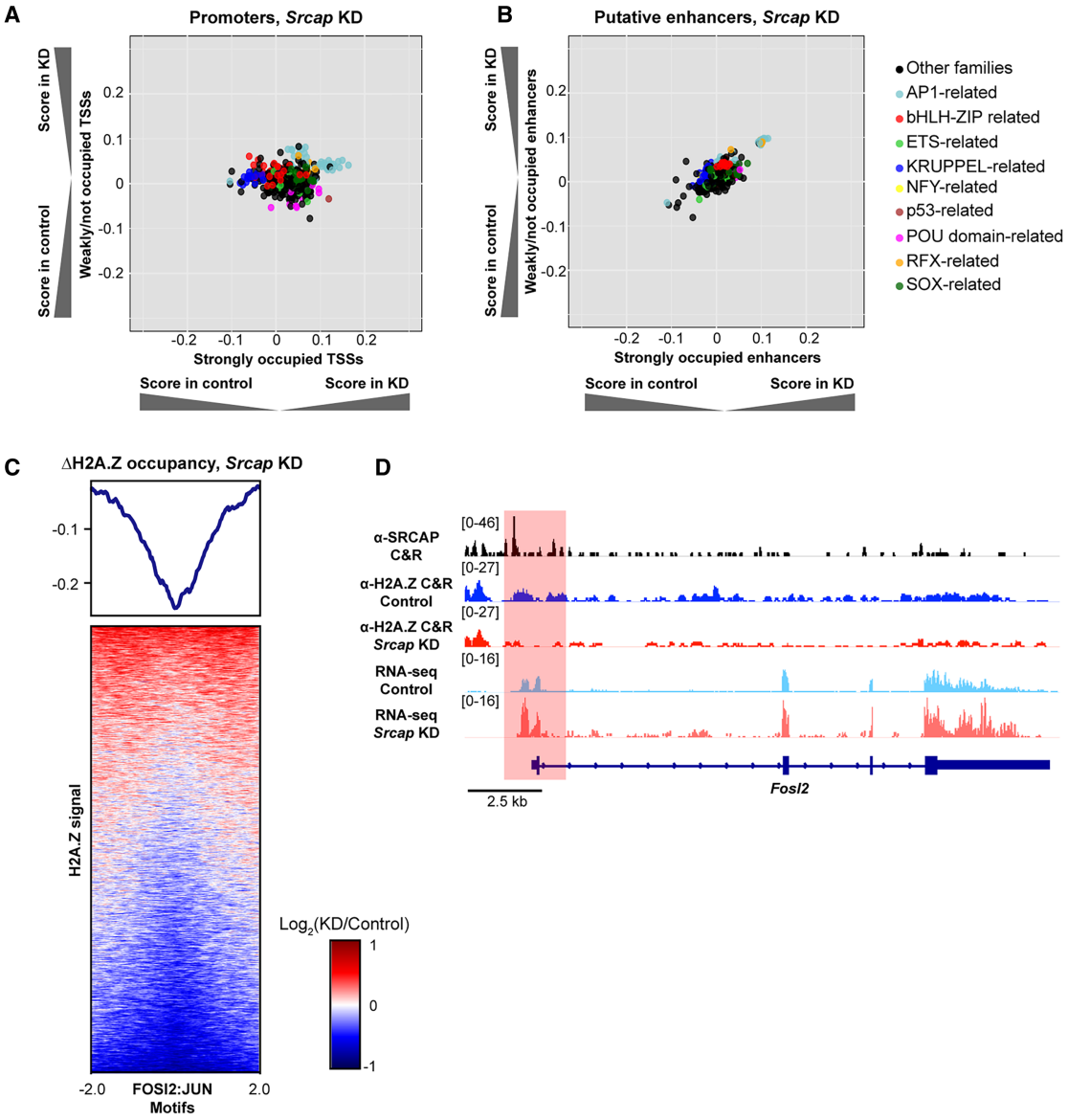

Figure 6. SRCAP regulates H2A.Z localization over AP-1 transcription factor binding sites

(A) Scatterplot comparing the binding score of different TF motifs at promoters bound versus not bound by SRCAP. Motifs representing factors from similar related groups are colored according to the legend. All factors shown have $p \leq 0.05$ at bound and unbound loci, defined from ATAC-seq data using TOBIAS.[80]

(B) As in (A) but for putative enhancers bound and unbound by SRCAP.

(C) Heatmap showing the change in H2A.Z binding over FOSL2:JUN motifs defined by JASPAR in the *Srcap* KD relative to control CUT&RUN experiments. n = 28,392 loci.

(D) Browser track showing chromatin accessibility (ATAC-seq) and comparing H2A.Z localization (CUT&RUN) and gene expression (RNA-seq) in control and *Srcap* KD at the *Fosl2* locus, which was differentially transcribed in *Srcap* depletion ($\log_2$(FC) = 1.04 and FDR = 3.3×10^{-7}). Red box indicates the promoter region.

remodelers with modest contributions to mRNA transcription regulation, including SMARCAL1, HLTF, and SHPRH, consistent with prior work where loss of each of these ATPases has been associated with effects on mRNA transcription in other systems.[35,37,42,55,97,98]

Our analyses suggest that this regulatory paradigm applies to both the coding and CRE-associated non-coding transcriptomes, with some notable distinctions. We observed altered transcription in all three classes of transcripts analyzed (mRNAs, uaRNAs, and eRNAs) in each depletion dataset, with the overall number of transcripts changed in each depletion remaining relatively proportional across all three classes. However, while 55% of mRNAs were significantly changed in only one remodeler depletion, only 27% of uaRNAs and 22% of putative eRNAs were changed in only one depletion. These findings suggest that remodelers are more collaborative in the

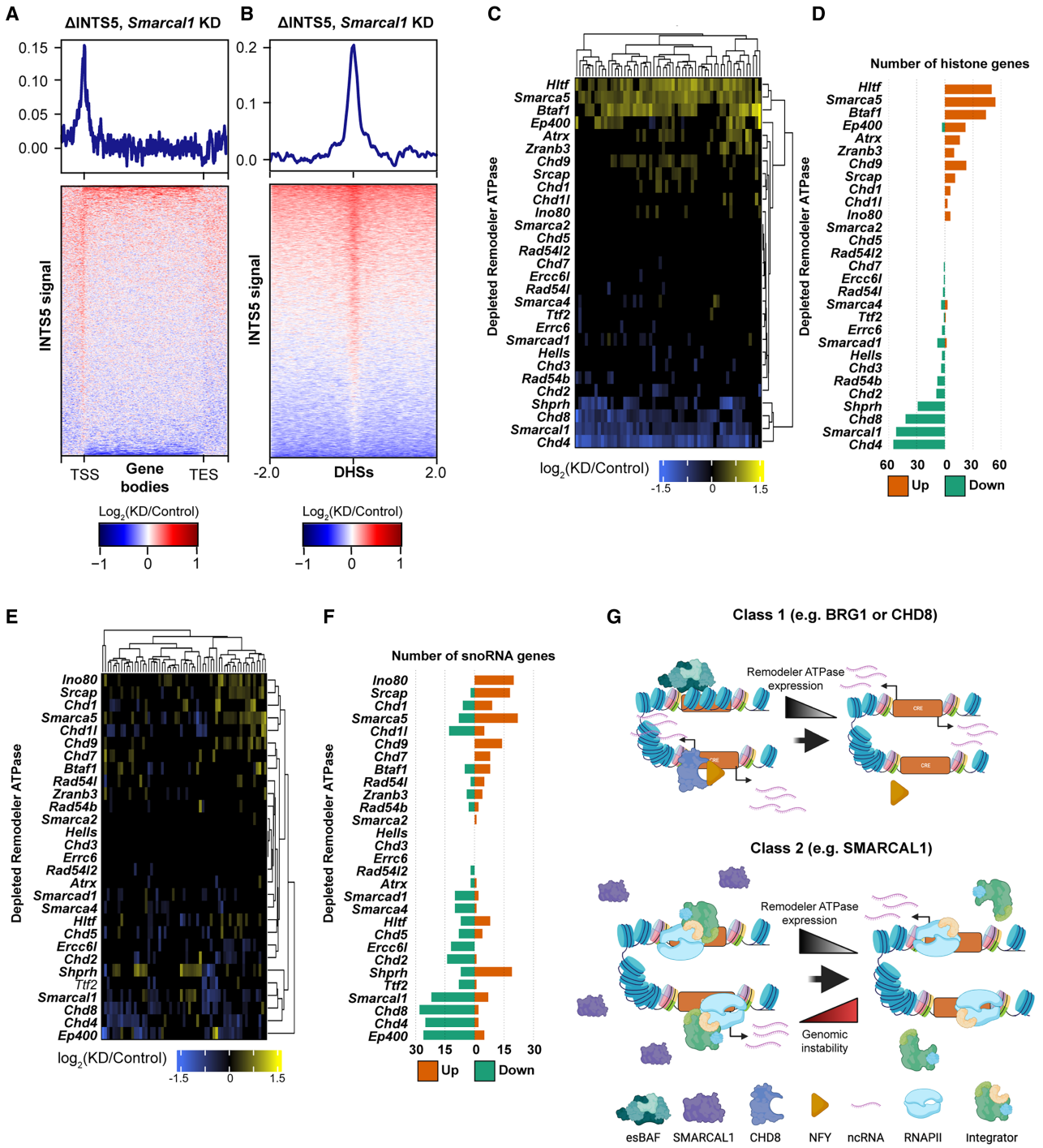

Figure 7. A subset of remodelers may have regulatory interactions with Integrator

(A) Heatmap showing the change in INTS5 localization (CUT&RUN) over mRNA gene bodies in *Smarcal1* KD relative to control. n = 22,598 loci.

(B) As in (A) but over putative enhancers. n = 101,588 loci.

(C) Heatmap showing the change in transcription of histone genes across all 29 TT-seq datasets (FDR $\leq$ 0.05). n = 58.

(D) Barplot quantifying the number of uaRNAs with increased (orange) or decreased (green) transcription in each depletion TT-seq dataset (FDR $\leq$ 0.05).

(E) As in (C) but for snoRNA genes. n = 61.

(F) As in (D) but for snoRNA genes.

(G) Model depicting two class mechanisms of transcription regulation by remodelers.

regulation of the non-coding transcriptome relative to the coding transcriptome.

Our data support BRG1 and BTAF1 acting as repressors of uaRNA transcription and suggest that several other remodelers, including HLTF, CHD1, and SNF2H, share in the repression of uaRNA in ES cells (Figure 2). We also observed remodelers operating as activators of uaRNA transcription, most notably CHD4, CHD8, and SMARCAL1. The predominant hypothesis for uaRNA function is currently that they contribute to the regulation of the corresponding mRNA. However, our findings (Figure 3), together with previous studies,[46,48,68,99,100] indicate that the regulation of the shared mRNA seems unlikely. Rather, we observe that uaRNAs are uniquely and independently regulated from the mRNAs for which they share a promoter.

Our analyses identified changes in enhancer transcription for many ATPase depletions, and we found that at least 16 depletions have corresponding changes in mRNA transcription (Figure 4). We have two non-mutually exclusive explanations for why our analyses predicted EPPs in only 16 remodeler depletions. First, many genes are likely regulated by multiple enhancers, and we were only able to detect transcriptional changes in mRNAs where the sole enhancer, primary enhancer, and/or multiple enhancers regulating the gene in question were perturbed upon ATPase depletion. Second, the elicited change in eRNA transcription from remodeler depletion was below our stringent significance threshold. Together, our data suggest that the depletion of several ATPases induces mRNA transcription associated with changes in enhancer activity in ES cells, including the now-identified contributors SRCAP, HLTF, SMARCAL1, BTAF1, SHPRH, and SMARCAD1.

Our mechanistic studies revealed that CHD8 and SRCAP act directly, while SMARCAL1 acts indirectly, on CRE-associated transcription (Figures 5, 6, and 7). Our data indicate that CHD8 orchestrates transcriptional changes in ES cells through the regulation of TFs, including ETS, p53, and NFY factors (Figure 5). Previously, homozygous deletion of CHD8 was associated with changes in chromatin accessibility in ES cells, whereas heterozygous deletion induced almost no detectable changes.[10] As a fraction of functional protein remains in the cell after our depletion approach, it is possible that we have not captured the full effects of this ATPase on chromatin accessibility. Another possible contributing factor is compensation by major regulators of accessibility, such as CHD4, BRG1, p400, and SNF2H, as has been recently demonstrated between mSWI/SNF and Tip60/p400 complexes.[95]

Our data support SRCAP contributing to transcriptome regulation through H2A.Z and AP-1 factors (Figure 6). Over 50% of H2A.Z peaks lost upon *Srcap* depletion were classified as strong enhancers or enhancers, while Tip60-p400 primarily localizes to promoters in ES cells.[6,44] This finding suggests a functional distinction between these two complexes, where Tip60-p400 targets H2A.Z to promoters while SRCAP loads H2A.Z at enhancers. Our data also show that loss of SRCAP results in a redistribution of H2A.Z to bivalent and repressed chromatin, indicating that SRCAP contributes to pluripotency in ES cells through the maintenance of proper H2A.Z localization. For both CHD8 and SRCAP, future studies using rapid depletion approaches, such as the dTAG or PROTAC systems, would help to inform their direct influences on the transcriptome.[101,102]

While our studies did not support the direct action of SMARCAL1 in CRE-associated transcription regulation, its depletion increased INTS5 recruitment at promoters and enhancers (Figure 7), suggesting that transcription changes result from defective post-transcriptional regulation. The Integrator complex is a multifaceted complex with roles in transcription termination, replication-dependent histone gene expression, snoRNA processing, and genomic stability.[89,90] Stressful growth conditions trigger genome-wide transcription termination defects[103,104] (similar to what has been seen upon rapid depletion of INTS11 in mouse ES cells[93]), de-regulation of uaRNA transcription,[63] and a decrease in interactions between Integrator complex subunits and RNA polymerase II.[105] Furthermore, loss of *Smarcal1* results in increased R-loop formation, and Integrator binds to regions with R-loops to resolve these structures to prevent DNA damage and replication stress.[106,107] We propose that the transcriptomic effects observed upon depletion of ATPases involved in genomic stability, such as SMARCAL1 and others, may be attributed, at least in part, to defective Integrator recruitment, binding, and/or activity, possibly due to increased R-loop accumulation. Therefore, remodelers can influence non-coding transcription at CREs through two mechanistic classes. Class 1 includes traditional mechanisms of regulation, such as regulation of chromatin accessibility, nucleosome positioning (i.e., BRG1), or TF occupancy (i.e., CHD8; Figure 7G). Class 2 includes indirect mechanisms of action, centered around the maintenance of genomic stability to limit stress responses and ensure transcriptional fidelity (i.e., SMARCAL1; Figure 7G). These mechanisms are not mutually exclusive, and future work is needed to define remodeler-Integrator interactions in transcription regulation.

Limitations of the study

Despite many attempts, we were unable to achieve depletion at or beyond 50% for three ATPases, *Chd6*, *Smarca1*, and *Ercc6l2*, and therefore, we did not continue with any experiments for these remodelers. Our transcriptomic screen was performed using endoribonuclease-digested short interfering RNA (esiRNA) depletion, which, despite resulting in robust depletion of the targeted remodeler, could have off-target effects. Furthermore, the 48 h depletion time point selected, while robust for depletion, is relatively long term compared to more recently used rapid depletion methods (such as dTAG and AID), meaning the transcriptomic changes observed are likely the result of both direct and indirect effects due to the remodeler depletion.

RESOURCE AVAILABILITY

Lead contact

All information and resource request for resources should be directed to the lead contact, Sarah J. Hainer (sarah.hainer@pitt.edu).

Materials availability

All unique materials and resources generated from this study are available upon request from the lead contact.

Data and code availability

- Raw data and processed files are available on GEO with accession GEO: GSE256314. Accession numbers are listed in the key resources table. This paper also used publicly available data. These accession numbers have been listed in the key resources table.
- All original code and data analyses have deposited on GitHub (https://github.com/bjp86/Patty_et_al_2024). The DOIs are listed in the key resources table.
- Any further needed information is available upon request from the lead contact.

ACKNOWLEDGMENTS

We thank Tom Fazzio and members of the Hainer Lab, especially Dave Klein and Rithika Sankar, for critical comments, discussion, and feedback regarding this article. This work was supported by NIH grant R35GM133732 (to S.J.H.) and NSF GRFP (to B.J.P.). This research was supported in part by the University of Pittsburgh Center for Research Computing (RRID: SCR_022735) through the resources provided. This work used the HTC cluster, which is supported by NIH award number S10OD028483. This project used the University of Pittsburgh HSCRF Genomics Research Core (RRID: SCR_018301) next-generation sequencing services, with special thanks to the assistant director, Will MacDonald.

AUTHOR CONTRIBUTIONS

Conceptualization, B.J.P. and S.J.H.; methodology, B.J.P., R.D., and S.J.H.; investigation, B.J.P., R.D., and S.J.H.; writing—original draft, B.J.P. and S.J.H.; writing—review & editing, B.J.P., R.D., and S.J.H.; funding acquisition, B.J.P. and S.J.H.; resources, S.J.H.; supervision, S.J.H.

DECLARATION OF INTERESTS

The authors declare no competing interests.

STAR★METHODS

Detailed methods are provided in the online version of this paper and include the following:

SUPPLEMENTAL INFORMATION

Supplemental information can be found online at https://doi.org/10.1016/j.celrep.2025.115767.

Received: February 28, 2024
Revised: March 14, 2025
Accepted: May 9, 2025

REFERENCES

1. Clapier, C.R., Iwasa, J., Cairns, B.R., and Peterson, C.L. (2017). Mechanisms of action and regulation of ATP-dependent chromatin-remodelling complexes. Nat. Rev. Mol. Cell Biol. *18*, 407–422.
2. Hargreaves, D.C., and Crabtree, G.R. (2011). ATP-dependent chromatin remodeling: Genetics, genomics and mechanisms. Cell Res. *21*, 396–420.
3. Eustermann, S., Patel, A.B., Hopfner, K.P., He, Y., and Korber, P. (2024). Energy-driven genome regulation by ATP-dependent chromatin remodellers. Nat. Rev. Mol. Cell Biol. *25*, 309–332.
4. Gourisankar, S., Krokhotin, A., Wenderski, W., and Crabtree, G.R. (2024). Context-specific functions of chromatin remodellers in development and disease. Nat. Rev. Genet. *25*, 340–361.
5. Nodelman, I.M., and Bowman, G.D. (2021). Biophysics of Chromatin Remodeling. Annu. Rev. Biophys. *50*, 73–93.
6. Fazzio, T.G., Huff, J.T., and Panning, B. (2008). An RNAi Screen of Chromatin Proteins Identifies Tip60-p400 as a Regulator of Embryonic Stem Cell Identity. Cell *134*, 162–174.
7. Zhao, H., Han, Z., Liu, X., Gu, J., Tang, F., Wei, G., and Jin, Y. (2017). The chromatin remodeler Chd4 maintains embryonic stem cell identity by controlling pluripotency- and differentiationassociated genes. J. Biol. Chem. *292*, 8507–8519.
8. Ho, L., Jothi, R., Ronan, J.L., Cui, K., Zhao, K., and Crabtree, G.R. (2009). An embryonic stem cell chromatin remodeling complex, esBAF, is an essential component of the core pluripotency transcriptional network. Proc. Natl. Acad. Sci. USA *106*, 5187–5191.
9. Gaspar-Maia, A., Alajem, A., Polesso, F., Sridharan, R., Mason, M.J., Heidersbach, A., Ramalho-Santos, J., McManus, M.T., Plath, K., Meshorer, E., and Ramalho-Santos, M. (2009). Chd1 regulates open chromatin and pluripotency of embryonic stem cells. Nature *460*, 863–868.
10. Sood, S., Weber, C.M., Hodges, H.C., Krokhotin, A., Shalizi, A., and Crabtree, G.R. (2020). CHD8 dosage regulates transcription in pluripotency and early murine neural differentiation. Proc. Natl. Acad. Sci. USA *117*, 22331–22340.
11. Barisic, D., Stadler, M.B., Iurlaro, M., and Schübeler, D. (2019). Mammalian ISWI and SWI/SNF selectively mediate binding of distinct transcription factors. Nature *569*, 136–140.
12. Xiao, S., Lu, J., Sridhar, B., Cao, X., Yu, P., Zhao, T., Chen, C.C., McDee, D., Sloofman, L., Wang, Y., et al. (2017). SMARCAD1 Contributes to the Regulation of Naive Pluripotency by Interacting with Histone Citrullination. Cell Rep. *18*, 3117–3128.
13. Semba, Y., Harada, A., Maehara, K., Oki, S., Meno, C., Ueda, J., Yamagata, K., Suzuki, A., Onimaru, M., Nogami, J., et al. (2017). Chd2 regulates chromatin for proper gene expression toward differentiation in mouse embryonic stem cells. Nucleic Acids Res. *45*, 8758–8772.
14. Wong, L.H., McGhie, J.D., Sim, M., Anderson, M.A., Ahn, S., Hannan, R.D., George, A.J., Morgan, K.A., Mann, J.R., and Choo, K.H.A. (2010). ATRX interacts with H3.3 in maintaining telomere structural integrity in pluripotent embryonic stem cells. Genome Res. *20*, 351–360.

15. Wang, L., Du, Y., Ward, J.M., Shimbo, T., Lackford, B., Zheng, X., Miao, Y.I., Zhou, B., Han, L., Fargo, D.C., et al. (2014). INO80 facilitates pluripotency gene activation in embryonic stem cell self-renewal, reprogramming, and blastocyst development. Cell Stem Cell *14*, 575–591.

16. Klein, D.C., Troy, K., Tripplehorn, S.A., and Hainer, S.J. (2023). The esBAF and ISWI nucleosome remodeling complexes influence occupancy of overlapping dinucleosomes and fragile nucleosomes in murine embryonic stem cells. BMC Genom. *24*, 201–216.

17. Sun, Z., and Bernstein, E. (2019). Histone variant macroH2A: from chromatin deposition to molecular function. Essays Biochem. *63*, 59–74.

18. Patty, B.J., and Hainer, S.J. (2020). Non-Coding RNAs and Nucleosome Remodeling Complexes: An Intricate Regulatory Relationship. Biology *9*, 213.

19. Preker, P., Nielsen, J., Kammler, S., Lykke-Andersen, S., Christensen, M. S., Mapendano, C.K., Schierup, M.H., and Jensen, T.H. (2008). RNA exosome depletion reveals transcription upstream of active human promoters. Science *322*, 1851–1854.

20. Preker, P., Almvig, K., Christensen, M.S., Valen, E., Mapendano, C.K., Sandelin, A., and Jensen, T.H. (2011). PROMoter uPstream Transcripts share characteristics with mRNAs and are produced upstream of all three major types of mammalian promoters. Nucleic Acids Res. *39*, 7179–7193.

21. Pefanis, E., Wang, J., Rothschild, G., Lim, J., Kazadi, D., Sun, J., Federation, A., Chao, J., Elliott, O., Liu, Z.P., et al. (2015). RNA exosome-regulated long non-coding RNA transcription controls super-enhancer activity. Cell *161*, 774–789.

22. Schaukowitch, K., Joo, J.Y., Liu, X., Watts, J.K., Martinez, C., and Kim, T. K. (2014). Enhancer RNA facilitates NELF release from immediate early genes. Mol. Cell *56*, 29–42.

23. Gorbovytska, V., Kim, S.K., Kuybu, F., Götze, M., Um, D., Kang, K., Pittroff, A., Brennecke, T., Schneider, L.M., Leitner, A., et al. (2022). Enhancer RNAs stimulate Pol II pause release by harnessing multivalent interactions to NELF. Nat. Commun. *13*, 2429.

24. Zhao, Y., Wang, L., Ren, S., Wang, L., Blackburn, P.R., McNulty, M.S., Gao, X., Qiao, M., Vessella, R.L., Kohli, M., et al. (2016). Activation of P-TEFb by Androgen Receptor-Regulated Enhancer RNAs in Castration-Resistant Prostate Cancer. Cell Rep. *15*, 599–610.

25. Tsai, P.F., Dell'Orso, S., Rodriguez, J., Vivanco, K.O., Ko, K.D., Jiang, K., Juan, A.H., Sarshad, A.A., Vian, L., Tran, M., et al. (2018). A Muscle-Specific Enhancer RNA Mediates Cohesin Recruitment and Regulates Transcription In trans. Mol. Cell *71*, 129–141.e8.

26. Rahnamoun, H., Lee, J., Sun, Z., Lu, H., Ramsey, K.M., Komives, E.A., and Lauberth, S.M. (2018). RNAs interact with BRD4 to promote enhanced chromatin engagement and transcription activation. Nat. Struct. Mol. Biol. *25*, 687–697.

27. Jiao, W., Chen, Y., Song, H., Li, D., Mei, H., Yang, F., Fang, E., Wang, X., Huang, K., Zheng, L., and Tong, Q. (2018). HPSE enhancer RNA promotes cancer progression through driving chromatin looping and regulating hnRNPU/p300/EGR1/HPSE axis. Oncogene *37*, 2728–2745.

28. Li, W., Notani, D., Ma, Q., Tanasa, B., Nunez, E., Chen, A.Y., Merkurjev, D., Zhang, J., Ohgi, K., Song, X., et al. (2013). Functional roles of enhancer RNAs for oestrogen-dependent transcriptional activation. Nature *498*, 516–520.

29. Yang, F., Tanasa, B., Micheletti, R., Ohgi, K.A., Aggarwal, A.K., and Rosenfeld, M.G. (2021). Shape of promoter antisense RNAs regulates ligand-induced transcription activation. Nature *595*, 444–449.

30. Wang, C., Jia, L., Wang, Y., Du, Z., Zhou, L., Wen, X., Li, H., Zhang, S., Chen, H., Chen, N., et al. (2020). Genome-wide interaction target profiling reveals a novel Peblr20-eRNA activation pathway to control stem cell pluripotency. Theranostics *10*, 353–370.

31. Alvarez-Dominguez, J.R., Knoll, M., Gromatzky, A.A., and Lodish, H.F. (2017). The Super-Enhancer-Derived alncRNA-EC7/Bloodlinc Potentiates Red Blood Cell Development in trans. Cell Rep. *19*, 2503–2514.

32. Liang, L., Cao, C., Ji, L., Cai, Z., Wang, D., Ye, R., Chen, J., Yu, X., Zhou, J., Bai, Z., et al. (2023). Complementary Alu sequences mediate enhancer–promoter selectivity. Nature *619*, 868–875.

33. Ye, B., Liu, B., Yang, L., Zhu, X., Zhang, D., Wu, W., Zhu, P., Wang, Y., Wang, S., Xia, P., et al. (2018). LncKdm2b controls self-renewal of embryonic stem cells via activating expression of transcription factor Zbtb3. EMBO J. *37*, 971744–e97215.

34. Giles, K.A., Gould, C.M., Du, Q., Skvortsova, K., Song, J.Z., Maddugoda, M.P., Achinger-Kawecka, J., Stirzaker, C., Clark, S.J., and Taberlay, P.C. (2019). Integrated epigenomic analysis stratifies chromatin remodellers into distinct functional groups. Epigenetics Chromatin *12*, 12–19.

35. Lee, D., An, J., Park, Y.U., Liaw, H., Woodgate, R., Park, J.H., and Myung, K. (2017). SHPRH regulates rRNA transcription by recognizing the histone code in an mTOR-dependent manner. Proc. Natl. Acad. Sci. USA *114*, E3424–E3433.

36. Ren, W., Medeiros, N., Warneford-Thomson, R., Wulfridge, P., Yan, Q., Bian, J., Sidoli, S., Garcia, B.A., Skordalakes, E., Joyce, E., et al. (2020). Disruption of ATRX-RNA interactions uncovers roles in ATRX localization and PRC2 function. Nat. Commun. *11*, 2219.

37. Gong, X., Kaushal, S., Ceccarelli, E., Bogdanova, N., Neville, C., Nguyen, T., Clark, H., Khatib, Z.A., Valentine, M., Look, A.T., and Rosenthal, N. (1997). Developmental regulation of Zbu1, a DNA-binding member of the SWI2/SNF2 family. Dev. Biol. *183*, 166–182.

38. Augello, M.A., Liu, D., Deonarine, L.D., Robinson, B.D., Huang, D., Stelloo, S., Blattner, M., Doane, A.S., Wong, E.W.P., Chen, Y., et al. (2019). CHD1 Loss Alters AR Binding at Lineage-Specific Enhancers and Modulates Distinct Transcriptional Programs to Drive Prostate Tumorigenesis. Cancer Cell *35*, 817–819.

39. Marques, J.G., Gryder, B.E., Pavlovic, B., Chung, Y., Ngo, Q.A., Frommelt, F., Gstaiger, M., Song, Y., Benischke, K., Laubscher, D., et al. (2020). NURD subunit CHD4 regulates super-enhancer accessibility in rhabdomyosarcoma and represents a general tumor dependency. Elife *9*, 549933–e55030.

40. Schnetz, M.P., Handoko, L., Akhtar-Zaidi, B., Bartels, C.F., Pereira, C.F., Fisher, A.G., Adams, D.J., Flicek, P., Crawford, G.E., Laframboise, T., et al. (2010). CHD7 targets active gene enhancer elements to modulate ES cell-specific gene expression. PLoS Genet. *6*, 10010233–e1001115.

41. Schnetz, M.P., Bartels, C.F., Shastri, K., Balasubramanian, D., Zentner, G.E., Balaji, R., Zhang, X., Song, L., Wang, Z., Laframboise, T., et al. (2009). Genomic distribution of CHD7 on chromatin tracks H3K4 methylation patterns. Genome Res. *19*, 590–601.

42. Bansal, R., Hussain, S., Chanana, U.B., Bisht, D., Goel, I., and Muthuswami, R. (2020). SMARCAL1, the annealing helicase and the transcriptional co-regulator. IUBMB Life *72*, 2080–2096.

43. Morris, S.A., Baek, S., Sung, M.H., John, S., Wiench, M., Johnson, T.A., Schiltz, R.L., and Hager, G.L. (2014). Overlapping chromatin-remodeling systems collaborate genome wide at dynamic chromatin transitions. Nat. Struct. Mol. Biol. *21*, 73–81.

44. De Dieuleveult, M., Yen, K., Hmitou, I., Depaux, A., Boussouar, F., Bou Dargham, D., Jounier, S., Humbertclaude, H., Ribierre, F., Baulard, C., et al. (2016). Genome-wide nucleosome specificity and function of chromatin remodellers in ES cells. Nature *530*, 113–116.

45. Yang, Y., Zhang, L., Xiong, C., Chen, J., Wang, L., Wen, Z., Yu, J., Chen, P., Xu, Y., Jin, J., et al. (2022). HIRA complex presets transcriptional potential through coordinating depositions of the histone variants H3.3 and H2A.Z on the poised genes in mESCs. Nucleic Acids Res. *50*, 191–206.

46. Xue, Y., Pradhan, S.K., Sun, F., Chronis, C., Tran, N., Su, T., Van, C., Vashisht, A., Wohlschlegel, J., Peterson, C.L., et al. (2017). Mot1, Ino80C, and NC2 Function Coordinately to Regulate Pervasive Transcription in Yeast and Mammals. Mol. Cell *67*, 594–607.e4.

47. Ceballos-Chávez, M., Subtil-Rodríguez, A., Giannopoulou, E.G., Soronellas, D., Vázquez-Chávez, E., Vicent, G.P., Elemento, O., Beato, M., and Reyes, J.C. (2015). The chromatin Remodeler CHD8 is required for

activation of progesterone receptor-dependent enhancers. PLoS Genet. *11*, e1005174.

48. Hainer, S.J., Gu, W., Carone, B.R., Landry, B.D., Rando, O.J., Mello, C. C., and Fazzio, T.G. (2015). Suppression of pervasive noncoding transcription in embryonic stem cells by esBAF. Genes Dev. *29*, 362–378.
49. Schwalb, B., Michel, M., Zacher, B., Frühauf, K., Demel, C., Tresch, A., Gagneur, J., and Cramer, P. (2016). TT-seq maps the human transient transcriptome. Science *352*, 1225–1228.
50. Frankish, A., Diekhans, M., Jungreis, I., Lagarde, J., Loveland, J.E., Mudge, J.M., Sisu, C., Wright, J.C., Armstrong, J., Barnes, I., et al. (2021). Gencode 2021. Nucleic Acids Res. *49*, D916–D923.
51. Kidder, B.L., Palmer, S., and Knott, J.G. (2009). SWI/SNF-Brg1 Regulates Self-Renewal and Occupies Core Pluripotency-Related Genes in Embryonic Stem Cells. Stem Cell. *27*, 317–328.
52. Weston, R., Peeters, H., and Ahel, D. (2012). ZRANB3 is a structure-specific ATP-dependent endonuclease involved in replication stress response. Genes Dev. *26*, 1558–1572.
53. Brühl, J., Trautwein, J., Schäfer, A., Linne, U., and Bouazoune, K. (2019). The DNA repair protein SHPRH is a nucleosome-stimulated ATPase and a nucleosome-E3 ubiquitin ligase. Epigenetics Chromatin *12*, 1–16.
54. Dhont, L., Mascaux, C., and Belayew, A. (2016). The helicase-like transcription factor (HLTF) in cancer: Loss of function or oncomorphic conversion of a tumor suppressor? Cell. Mol. Life Sci. *73*, 129–147.
55. Pugliese, G.M., Salaris, F., Palermo, V., Marabitti, V., Morina, N., Rosa, A., Franchitto, A., and Pichierri, P. (2019). Inducible SMARCAL1 knockdown in iPSC reveals a link between replication stress and altered expression of master differentiation genes. Dis. Model. Mech. *12*, dmm039487.
56. Mohd-Sarip, A., Teeuwssen, M., Bot, A.G., De Herdt, M.J., Willems, S. M., Baatenburg de Jong, R.J., Looijenga, L.H.J., Zatreanu, D., Bezstarosti, K., van Riet, J., et al. (2017). DOC1-Dependent Recruitment of NURD Reveals Antagonism with SWI/SNF during Epithelial-Mesenchymal Transition in Oral Cancer Cells. Cell Rep. *20*, 61–75.
57. Pundhir, S., Su, J., Tapia, M., Hansen, A.M., Haile, J.S., Hansen, K., and Porse, B.T. (2023). The impact of SWI/SNF and NuRD inactivation on gene expression is tightly coupled with levels of RNA polymerase II occupancy at promoters. Genome Res. *33*, 332–345.
58. Chronis, C., Fiziev, P., Papp, B., Butz, S., Bonora, G., Sabri, S., Ernst, J., and Plath, K. (2017). Cooperative Binding of Transcription Factors Orchestrates Reprogramming. Cell *168*, 442–459.e20.
59. Harikumar, A., and Meshorer, E. (2015). Chromatin remodeling and bivalent histone modifications in embryonic stem cells. EMBO Rep. *16*, 1609–1619.
60. Creyghton, M.P., Markoulaki, S., Levine, S.S., Hanna, J., Lodato, M.A., Sha, K., Young, R.A., Jaenisch, R., and Boyer, L.A. (2008). H2AZ Is Enriched at Polycomb Complex Target Genes in ES Cells and Is Necessary for Lineage Commitment. Cell *135*, 649–661.
61. Ho, L., Miller, E.L., Ronan, J.L., Ho, W.Q., Jothi, R., and Crabtree, G.R. (2011). EsBAF facilitates pluripotency by conditioning the genome for LIF/STAT3 signalling and by regulating polycomb function. Nat. Cell Biol. *13*, 903–913.
62. Yang, F. (2022). Promoter antisense RNAs: beyond transcription byproducts of active promoters. RNA Biol. *19*, 533–540.
63. Lloret-Llinares, M., Mapendano, C.K., Martlev, L.H., Lykke-Andersen, S., and Jensen, T.H. (2016). Relationships between PROMPT and gene expression. RNA Biol. *13*, 6–14.
64. Whitehouse, I., Rando, O.J., Delrow, J., and Tsukiyama, T. (2007). Chromatin remodelling at promoters suppresses antisense transcription. Nature *450*, 1031–1035.
65. Hennig, B.P., Bendrin, K., Zhou, Y., and Fischer, T. (2012). Chd1 chromatin remodelers maintain nucleosome organization and repress cryptic transcription. EMBO Rep. *13*, 997–1003.
66. Marquardt, S., Escalante-Chong, R., Pho, N., Wang, J., Churchman, L.S., Springer, M., and Buratowski, S. (2014). A chromatin-based mechanism for limiting divergent noncoding transcription. Cell *157*, 1712–1723.
67. Haokip, D.T., Goel, I., Arya, V., Sharma, T., Kumari, R., Priya, R., Singh, M., and Muthuswami, R. (2016). Transcriptional Regulation of Atp-Dependent Chromatin Remodeling Factors: Smarcal1 and Brg1 Mutually Co-Regulate Each Other. Sci. Rep. *6*, 20532–20613.
68. Flynn, R.A., Almada, A.E., Zamudio, J.R., and Sharp, P.A. (2011). Antisense RNA polymerase II divergent transcripts are P-TEFb dependent and substrates for the RNA exosome. Proc. Natl. Acad. Sci. USA *108*, 10460–10465.
69. ENCODE Project Consortium (2012). An integrated encyclopedia of DNA elements in the human genome. Nature *489*, 57–74.
70. Peng, T., Zhai, Y., Atlasi, Y., Ter Huurne, M., Marks, H., Stunnenberg, H. G., and Megchelenbrink, W. (2020). STARR-seq identifies active, chromatin-masked, and dormant enhancers in pluripotent mouse embryonic stem cells. Genome Biol. *21*, 243–327.
71. Mantsoki, A., Parussel, K., and Joshi, A. (2021). Identification and Characterisation of Putative Enhancer Elements in Mouse Embryonic Stem Cells. Bioinf. Biol. Insights *15*, 1177932220974623.
72. Hsieh, T.H.S., Cattoglio, C., Slobodyanyuk, E., Hansen, A.S., Darzacq, X., and Tjian, R. (2022). Enhancer–promoter interactions and transcription are largely maintained upon acute loss of CTCF, cohesin, WAPL or YY1. Nat. Genet. *54*, 1919–1932.
73. Sahlén, P., Abdullayev, I., Ramsköld, D., Matskova, L., Rilakovic, N., Lötstedt, B., Albert, T.J., Lundeberg, J., and Sandberg, R. (2015). Genome-wide mapping of promoter-anchored interactions with close to single-enhancer resolution. Genome Biol. *16*, 156.
74. Cairns, J., Freire-Pritchett, P., Wingett, S.W., Várnai, C., Dimond, A., Plagnol, V., Zerbino, D., Schoenfelder, S., Javierre, B.M., Osborne, C., et al. (2016). CHiCAGO: Robust detection of DNA looping interactions in Capture Hi-C data. Genome Biol. *17*, 127–217.
75. Schoenfelder, S., Mifsud, B., Senner, C.E., Todd, C.D., Chrysanthou, S., Darbo, E., Hemberger, M., and Branco, M.R. (2018). Divergent wiring of repressive and active chromatin interactions between mouse embryonic and trophoblast lineages. Nat. Commun. *9*, 4189.
76. Zhou, B., Wang, L., Zhang, S., Bennett, B.D., He, F., Zhang, Y., Xiong, C., Han, L., Diao, L., Li, P., et al. (2016). INO80 governs superenhancer-mediated oncogenic transcription and tumor growth in melanoma. Genes Dev. *30*, 1440–1453.
77. Uyehara, C.M., and Apostolou, E. (2023). 3D enhancer-promoter interactions and multi-connected hubs: Organizational principles and functional roles. Cell Rep. *42*, 112068.
78. Jin, F., Li, Y., Dixon, J.R., Selvaraj, S., Ye, Z., Lee, A.Y., Yen, C.A., Schmitt, A.D., Espinoza, C.A., and Ren, B. (2013). A high-resolution map of the three-dimensional chromatin interactome in human cells. Nature *503*, 290–294.
79. Sanyal, A., Lajoie, B.R., Jain, G., and Dekker, J. (2012). The long-range interaction landscape of gene promoters. Nature *489*, 109–113.
80. Bentsen, M., Goymann, P., Schultheis, H., Klee, K., Petrova, A., Wiegandt, R., Fust, A., Preussner, J., Kuenne, C., Braun, T., et al. (2020). ATAC-seq footprinting unravels kinetics of transcription factor binding during zygotic genome activation. Nat. Commun. *11*, 4267.
81. Haddad Derafshi, B., Danko, T., Chanda, S., Batista, P.J., Litzenburger, U., Lee, Q.Y., Ng, Y.H., Sebin, A., Chang, H.Y., Südhof, T.C., and Wernig, M. (2022). The autism risk factor CHD8 is a chromatin activator in human neurons and functionally dependent on the ERK-MAPK pathway effector ELK1. Sci. Rep. *12*, 22425–22428.
82. Nita, A., Muto, Y., Katayama, Y., Matsumoto, A., Nishiyama, M., and Nakayama, K.I. (2021). The autism-related protein CHD8 contributes to the stemness and differentiation of mouse hematopoietic stem cells. Cell Rep. *34*, 108688.

83. Nishiyama, M., Oshikawa, K., Tsukada, Y.i., Nakagawa, T., Iemura, S.i., Natsume, T., Fan, Y., Kikuchi, A., Skoultchi, A.I., and Nakayama, K.I. (2009). CHD8 suppresses p53-mediated apoptosis through histone H1 recruitment during early embryogenesis. Nat. Cell Biol. *11*, 172–182.

84. Pintacuda, G., Wei, G., Roustan, C., Kirmizitas, B.A., Solcan, N., Cerase, A., Castello, A., Mohammed, S., Moindrot, B., Nesterova, T.B., and Brockdorff, N. (2017). hnRNPK Recruits PCGF3/5-PRC1 to the Xist RNA B-Repeat to Establish Polycomb-Mediated Chromosomal Silencing. Mol. Cell *68*, 955–969.e10.

85. Ruhl, D.D., Jin, J., Cai, Y., Swanson, S., Florens, L., Washburn, M.P., Conaway, R.C., Conaway, J.W., and Chrivia, J.C. (2006). Purification of a human SRCAP complex that remodels chromatin by incorporating the histone variant H2A.Z into nucleosomes. Biochemistry *45*, 5671–5677.

86. Wong, M.M., Cox, L.K., and Chrivia, J.C. (2007). The chromatin remodeling protein, SRCAP, is critical for deposition of the histone variant H2A.Z at promoters. J. Biol. Chem. *282*, 26132–26139.

87. Cole, L., Kurscheid, S., Nekrasov, M., Domaschenz, R., Vera, D.L., Dennis, J.H., and Tremethick, D.J. (2021). Multiple roles of H2A.Z in regulating promoter chromatin architecture in human cells. Nat. Commun. *12*, 2524–2615.

88. O'Donnell, A., Yang, S.H., and Sharrocks, A.D. (2013). PARP1 orchestrates variant histone exchange in signal-mediated transcriptional activation. EMBO Rep. *14*, 1084–1091.

89. Wagner, E.J., Tong, L., and Adelman, K. (2023). Integrator is a global promoter-proximal termination complex. Mol. Cell *83*, 416–427.

90. Mendoza-Figueroa, M.S., Tatomer, D.C., and Wilusz, J.E. (2020). The Integrator Complex in Transcription and Development. Trends Biochem. Sci. *45*, 923–934.

91. Rouvière, J.O., Lykke-Andersen, S., and Jensen, T.H. (2022). Control of non-productive RNA polymerase II transcription via its early termination in metazoans. Biochem. Soc. Trans. *50*, 283–295.

92. Lai, F., Gardini, A., Zhang, A., and Shiekhattar, R. (2015). Integrator mediates the biogenesis of enhancer RNAs. Nature *525*, 399–403.

93. Stein, C.B., Field, A.R., Mimoso, C.A., Zhao, C., Huang, K.L., Wagner, E. J., and Adelman, K. (2022). Integrator endonuclease drives promoter-proximal termination at all RNA polymerase II-transcribed loci. Mol. Cell *82*, 4232–4245.e11.

94. Lykke-Andersen, S., Žumer, K., Molska, E.Š., Rouvière, J.O., Wu, G., Demel, C., Schwalb, B., Schmid, M., Cramer, P., and Jensen, T.H. (2021). Integrator is a genome-wide attenuator of non-productive transcription. Mol. Cell *81*, 514–529.e6. https://doi.org/10.1016/j.molcel.2020.12.014.

95. Martin, B.J.E., Ablondi, E.F., Goglia, C., Mimoso, C.A., Espinel-Cabrera, P.R., and Adelman, K. (2023). Global identification of SWI/SNF targets reveals compensation by EP400. Cell *186*, 5290–5307.e26.

96. Choukrallah, M.A., Kobi, D., Martianov, I., Pijnappel, W.W.M.P., Mischerikow, N., Ye, T., Heck, A.J.R., Timmers, H.T.M., and Davidson, I. (2012). Interconversion between active and inactive TATA-binding protein transcription complexes in the mouse genome. Nucleic Acids Res. *40*, 1446–1459.

97. Elserafy, M., Abugable, A.A., Atteya, R., and El-Khamisy, S.F. (2018). Rad5, HLTF, and SHPRH: A Fresh View of an Old Story. Trends Genet. *34*, 574–577.

98. Yang, B., Xu, X., Russell, L., Sullenberger, M.T., Yanowitz, J.L., and Maine, E.M. (2019). A DNA repair protein and histone methyltransferase interact to promote genome stability in the Caenorhabditis elegans germ line. PLoS Genet. *15*, 10079922–e1008029.

99. Wu, A.C.K., Patel, H., Chia, M., Moretto, F., Frith, D., Snijders, A.P., and van Werven, F.J. (2018). Repression of Divergent Noncoding Transcription by a Sequence-Specific Transcription Factor. Mol. Cell *72*, 942–954.e7.

100. Almada, A.E., Wu, X., Kriz, A.J., Burge, C.B., and Sharp, P.A. (2013). Promoter directionality is controlled by U1 snRNP and polyadenylation signals. Nature *499*, 360–363.

101. Nabet, B., Roberts, J.M., Buckley, D.L., Paulk, J., Dastjerdi, S., Yang, A., Leggett, A.L., Erb, M.A., Lawlor, M.A., Souza, A., et al. (2018). The dTAG system for immediate and target-specific protein degradation. Nat. Chem. Biol. *14*, 431–441.

102. Sakamoto, K.M., Kim, K.B., Kumagai, A., Mercurio, F., Crews, C.M., and Deshaies, R.J. (2001). Protacs: Chimeric molecules that target proteins to the Skp1-Cullin-F box complex for ubiquitination and degradation. Proc. Natl. Acad. Sci. USA *98*, 8554–8559.

103. Vilborg, A., Passarelli, M.C., Yario, T.A., Tycowski, K.T., and Steitz, J.A. (2015). Widespread Inducible Transcription Downstream of Human Genes. Mol. Cell *59*, 449–461.

104. Mahat, D.B., Salamanca, H.H., Duarte, F.M., Danko, C.G., and Lis, J.T. (2016). Mammalian Heat Shock Response and Mechanisms Underlying Its Genome-wide Transcriptional Regulation. Mol. Cell *62*, 63–78.

105. Rosa-Mercado, N.A., Zimmer, J.T., Apostolidi, M., Rinehart, J., Simon, M.D., and Steitz, J.A. (2021). Hyperosmotic stress alters the RNA polymerase II interactome and induces readthrough transcription despite widespread transcriptional repression. Mol. Cell *81*, 502–513.e4.

106. Hodson, C., van Twest, S., Dylewska, M., O'Rourke, J.J., Tan, W., Murphy, V.J., Walia, M., Abbouche, L., Nieminuszczy, J., Dunn, E., et al. (2022). Branchpoint translocation by fork remodelers as a general mechanism of R-loop removal. Cell Rep. *41*, 111749.

107. Bhowmick, R., Mehta, K.P.M., Lerdrup, M., and Cortez, D. (2023). Integrator facilitates RNAPII removal to prevent transcription-replication collisions and genome instability. Mol. Cell *83*, 2357–2366.e8.

108. Hooper, M., Hardy, K., Handyside, A., Hunter, S., and Mock, M. (1987). HPRT-deficient (Lesch–Nyhan) mouse embryos derived from germline colonization by cultured cells. Nature *326*, 292–295. https://doi.org/10.1038/326292a0.

109. Sancak, Y., Peterson, T.R., Shaul, Y.D., Lindquist, R.A., Thoreen, C.C., Bar-Peled, L., and Sabatini, D.M. (2008). The rag GTPases bind raptor and mediate amino acid signaling to mTORC1. Science *320*, 1496–1501.

110. Henschel, A., Buchholz, F., and Habermann, B. (2004). DEQOR: A web-based tool for the design and quality control of siRNAs. Nucleic Acids Res. *32*, 113–120.

111. Bolger, A.M., Lohse, M., and Usadel, B. (2014). Trimmomatic: A flexible trimmer for Illumina sequence data. Bioinformatics *30*, 2114–2120.

112. Martin, M. (2011). Cutadapt removes adapter sequences from high-throughput sequencing reads. EMBnet. j. *17*, 10.

113. Dobin, A., Davis, C.A., Schlesinger, F., Drenkow, J., Zaleski, C., Jha, S., Batut, P., Chaisson, M., and Gingeras, T.R. (2013). STAR: Ultrafast universal RNA-seq aligner. Bioinformatics *29*, 15–21.

114. Li, H., and Durbin, R. (2009). Fast and accurate short read alignment with Burrows-Wheeler transform. Bioinformatics *25*, 1754–1760.

115. Liao, Y., Smyth, G.K., and Shi, W. (2014). FeatureCounts: An efficient general purpose program for assigning sequence reads to genomic features. Bioinformatics *30*, 923–930.

116. Zhang, Y., Parmigiani, G., and Johnson, W.E. (2020). ComBat-seq: Batch effect adjustment for RNA-seq count data. NAR Genom. Bioinform. *2*. lqaa078–10.

117. Love, M.I., Huber, W., and Anders, S. (2014). Moderated estimation of fold change and dispersion for RNA-seq data with DESeq2. Genome Biol. *15*, 550–621.

118. Wu, T., Hu, E., Xu, S., Chen, M., Guo, P., Dai, Z., Feng, T., Zhou, L., Tang, W., Zhan, L., et al. (2021). clusterProfiler 4.0: A universal enrichment tool for interpreting omics data. Innovation *2*, 100141.

119. Ramírez, F., Dündar, F., Diehl, S., Grüning, B.A., and Manke, T. (2014). DeepTools: A flexible platform for exploring deep-sequencing data. Nucleic Acids Res. *42*, W187–W191.

120. Robinson, J.T., Thorvaldsdóttir, H., Winckler, W., Guttman, M., Lander, E.S., Getz, G., and Mesirov, J.P. (2011). Integrative genomics viewer. Nat. Biotechnol. *29*, 24–26.

121. Quinlan, A.R., and Hall, I.M. (2010). BEDTools: A flexible suite of utilities for comparing genomic features. Bioinformatics *26*, 841–842.

122. Smith, J.P., Corces, M.R., Xu, J., Reuter, V.P., Chang, H.Y., and Sheffield, N.C. (2021). PEPATAC: An optimized pipeline for ATAC-seq data analysis with serial alignments. NAR Genom. Bioinform. *3*. lqab101–9.

123. Langmead, B., and Salzberg, S.L. (2012). Fast gapped-read alignment with Bowtie 2. Nat. Methods *9*, 357–359.

124. Zhang, Y., Liu, T., Meyer, C.A., Eeckhoute, J., Johnson, D.S., Bernstein, B.E., Nusbaum, C., Myers, R.M., Brown, M., Li, W., and Liu, X.S. (2008). Model-based analysis of ChIP-Seq (MACS). Genome Biol. *9*, R137.

125. Broad Institute (2009). Picard Tools - By Broad Institute. Github. https://broadinstitute.github.io/picard/.

126. Robinson, M.D., McCarthy, D.J., and Smyth, G.K. (2010). edgeR: A Bioconductor package for differential expression analysis of digital gene expression data. Bioinformatics *26*, 139–140.

127. Risso, D., Ngai, J., Speed, T.P., and Dudoit, S. (2014). Normalization of RNA-seq data using factor analysis of control genes or samples. Nat. Biotechnol. *32*, 896–902.

128. Yang, D., Buchholz, F., Huang, Z., Goga, A., Chen, C.Y., Brodsky, F.M., and Bishop, J.M. (2002). Short RNA duplexes produced by hydrolysis with Escherichia coli RNase III mediate effective RNA interference in mammalian cells. Proc. Natl. Acad. Sci. USA *99*, 9942–9947.

129. Rao, X., Huang, X., Zhou, Z., and Lin, X. (2013). An improvement of the 2^ (-delta delta CT) method for quantitative real-time polymerase chain reaction data analysis. Biostat. Bioinforma. Biomath. *3*, 71–85.

130. Klein, D.C., Lardo, S.M., McCannell, K.N., and Hainer, S.J. (2022). FACT regulates pluripotency through distal regulation of gene expression in murine embryonic stem cells. Preprint at bioRxiv. https://doi.org/10.1186/s12915-023-01669-0.

131. Klein, D.C., Lardo, S.M., and Hainer, S.J. (2024). The ncBAF complex regulates transcription in AML through H3K27ac sensing by BRD9. Cancer Res. Commun. *4*, 237–252.

132. Lardo, S.M., and Hainer, S.J. (2022). Single-Cell Factor Localization on Chromatin using Ultra-Low Input Cleavage Under Targets and Release using Nuclease. JoVE J. e63536. https://doi.org/10.3791/63536.

133. Patty, B.J., and Hainer, S.J. (2021). Transcription factor chromatin profiling genome-wide using uliCUT& RUN in single cells and individual blastocysts. Nat. Protoc. *16*, 2633–2666.

134. Yue, F., Cheng, Y., Breschi, A., Vierstra, J., Wu, W., Ryba, T., Sandstrom, R., Ma, Z., Davis, C., Pope, B.D., et al. (2014). A comparative encyclopedia of DNA elements in the mouse genome. Nature *515*, 355–364.

135. Li, H., Handsaker, B., Wysoker, A., Fennell, T., Ruan, J., Homer, N., Marth, G., Abecasis, G., and Durbin, R.; 1000 Genome Project Data Processing Subgroup (2009). The Sequence Alignment/Map format and SAMtools. Bioinformatics *25*, 2078–2079.

136. Heger, A., Webber, C., Goodson, M., Ponting, C.P., and Lunter, G. (2013). GAT: A simulation framework for testing the association of genomic intervals. Bioinformatics *29*, 2046–2048.

137. Castro-Mondragon, J.A., Riudavets-Puig, R., Rauluseviciute, I., Lemma, R.B., Turchi, L., Blanc-Mathieu, R., Lucas, J., Boddie, P., Khan, A., Manosalva Pérez, N., et al. (2022). JASPAR 2022: The 9th release of the open-access database of transcription factor binding profiles. Nucleic Acids Res. *50*, D165–D173.

STAR★METHODS

KEY RESOURCES TABLE

REAGENT or RESOURCE	SOURCE	IDENTIFIER
Antibodies		
Rabbit polyclonal anti-SRCAP	Kerafast	ESL103; RRID: AB_3086743
Rabbit polyclonal anti-SMARCAL1	Invitrogen	PA5-28980; RRID:AB_2546456
Mouse monoclonal Anti-IgG	Sigma-Aldrich	06-371; RRID:AB_11210670
Rabbit polyclonal anti-H3K27ac	abcam	ab4729; RRID:AB_2118291
Rabbit polyclonal anti-H2A.Z	abcam	ab4174; RRID:AB_304345
Mouse monoclonal anti-NFYA	Santa Cruz	SC-17753; RRID:AB_628018
Rabbit polyclonal anti-INTS5	Proteintech	14069-1-AP; RRID:AB_2296187
Rabbit polyclonal anti-CHD1	Diagenode	C15410334; RRID:AB_3107183
Mouse monoclonal anti-CHD4	abcam	ab70469; RRID:AB_2229454
Rabbit polyclonal anti-CHD8	NOVUS	nb10060418; RRID:AB_905325
Rabbit polyclonal anti-BRG1	Bethyl	A300-813A; RRID:AB_2191850
Rabbit polyclonal anti-BTAF1	abcam	ab72285; RRID:AB_1271174
Rabbit monoclonal anti-CHD2	Invitrogen	MA5-47275; RRID:AB_2938347
Rabbit polyclonal anti-INO80	Invitrogen	PA5-65296; RRID:AB_2665135
Rabbit polyclonal anti-SNF2H	Invitrogen	PA5-52601; RRID:AB_2647608
Rabbit polyclonal anti-SMARCAD1	Invitrogen	PA5-53482; RRID:AB_2647609
Mouse monoclonal anti-V5	Invitrogen	R960-25; RRID:AB_2556564
Bacterial and virus strains		
(Left blank intentionally)		
Biological samples		
(Left blank intentionally)		
Chemicals, peptides, and recombinant proteins		
DMEM base medium	Sigma Aldrich	D6546-500mL
nonessential amino acids	Corning	25-025-CI
L-glutamine	Corning	25-005-CI
β-mercaptoethanol	Acros Organics	EW-88124-66
Trypsin	Corning	25-052-CI
dNTPs	NEB	N0447L
10X Thermo PCR buffer	NEB	B9004S
Taq Polymerase	NEB	M0267X
Shortcut RNase III	NEB	M0245L
FuGene HD	Promega	E2311
T7 polymerase	This paper	In house
Lipofectamine 3000	Invitrogen	L3000-015
OptiMEM media	Gibco	31985–070
Random Hexamers	Promega	C118A
First Strand buffer	Invitrogen	Y02321
2X SYBR GREEN	KAPA Biosystems	KK4601
Trizol	Invitrogen	15596018
4-thio-uridine (4sU)	Carbosynth	T4509
EZ-Link HPDP-Biotin	ThermoFisher	21341
Streptavidin C1 beads	Invitrogen	65001

(*Continued on next page*)

Continued

REAGENT or RESOURCE	SOURCE	IDENTIFIER
RNase H	McLab	RNHE-100
10X RNase H buffer	McLab	B-RH10
Turbo DNase	Invitrogen	AM2238
10X Turbo DNase buffer	Invitrogen	4022G
Superscript III	Invitrogen	56575
AMPure XP beads	Beckman Coulter	A63881
10X Buffer 2	NEB	B7002S
DNA Polymerase I	NEB	M0209L
10X T4 DNA Ligase buffer	NEB	B0202A
T4 DNA Polymerase	NEB	M0203L
Klenow 3′ to 5′ exo	NEB	M0212L
2X Quick Ligase buffer	NEB	M2200L
T4 DNA ligase	NEB	M0202L
USER enzyme	NEB	M5505L
5X HF Phusion buffer	NEB	F-518
Phusion Polymerase	NEB	01046976
pA/pAG-Mnase	This paper	In house
Lectin-coated concanavalin beads	Polysciences	86057–10
Protease inhibitors	Pierce	A32965
RNase A	Invitrogen	2845880
Proteinase K	Meridian	BIO-37084
5X KAPA HF buffer	KAPABiosystems	KB2500
2X Tagmentation buffer	Diagenode	C01019043
Preloaded Tn5 Tagmentase	Diagenode	C01070012-30
Critical commercial assays		
Qubit RNA broad range quantification kit	ThermoFisher	Q10210
Quibit RNA High Sensitivity quantification kit	ThermoFisher	Q32852
Quibit dsDNA High Sensitivity Kit	ThermoFisher	Q32851
RNA clean and concentrator kit	Zymo Research	R1018
PureLink RNA Mini Kit	Invitrogen	12183025
DNA Clean and Concentrator Kit	Zymo Research	D4004
Ultra II RNA Library prep kit	NEB	E7770L
Deposited data		
GEO accession: GSE256314	This paper	https://www.ncbi.nlm.nih.gov/geo/query/acc.cgi?acc=GSE256314
Experimental models: Cell lines		
ES-E14TG2a (E14) embryonic stem cells	Jackson Laboratories	RRID:CVCL9108[108]
Experimental models: Organisms/strains		
(Left blank intentionally)		
Oligonucleotides		
esiRNA primer sequences	This paper	See Table S4
RT-qPCR primer sequences	This paper	See Table S4
sgRNA sequences	This paper	See Table S4
Homology constructs	This paper	See Table S4
Plasmid: pLJM1-EGFP for GFP esiRNA generation	Sancak et al.[109]	Addgene plasmid #19319
Recombinant DNA		
(Left blank intentionally)		

(*Continued on next page*)

Continued

REAGENT or RESOURCE	SOURCE	IDENTIFIER
Software and algorithms		
DEQOR	Henschel et al.[110]	https://www.eupheria.com/tools-resources/deqor/
trimmomatic	Bolger et al.[111]	http://www.usadellab.org/cms/?page=trimmomatic
cutadapt	Martin[112]	https://cutadapt.readthedocs.io/en/stable/
STAR	Dobin et al.[113]	https://github.com/alexdobin/STAR
SAMtools	Li and Durbin[114]	https://www.htslib.org/
featurecounts	Liao et al.[115]	https://subread.sourceforge.net/
R (version 4.0.0)	R project	https://www.r-project.org/
Combat-seq R package	Zhang et al.[116]	https://www.bioconductor.org/packages/release/bioc/html/sva.html
DEseq2 R package	Love and Anders[117]	https://bioconductor.org/packages/release/bioc/html/DESeq2.html
clusterProfiler R package	Wu et al.[118]	https://bioconductor.org/packages/release/bioc/html/clusterProfiler.html
deepTools	Ramirez et al.[119]	https://deeptools.readthedocs.io/en/develop/content/list_of_tools.html
IGV	Robinson et al.[120]	https://www.igv.org
bedtools[121]	Quinlin and Hall[121]	https://bedtools.readthedocs.io/en/latest/
Pepatac	Smith et al.[122]	https://pepatac.databio.org/en/latest/
Bowtie2	Langmead and Salzburg[123]	https://bowtie-bio.sourceforge.net/bowtie2/index.shtml
MACS2	Zhang et al.[124]	https://pypi.org/project/MACS2/
Picard	Broad Institute[125]	https://broadinstitute.github.io/picard/
edgeR R package	Robison et al.[126]	https://bioconductor.org/packages/release/bioc/html/edgeR.html
RUVseq R package	Risso et al.[127]	https://bioconductor.org/packages/release/bioc/html/RUVSeq.html
TOBIAS	Betsen et al.[80]	https://github.com/loosolab/TOBIAS
Scripts and data analysis	This paper	https://github.com/bjp86/Patty_et_al_2024 https://doi.org/10.5281/zenodo.15298299
Other		
(Left blank intentionally)		

EXPERIMENTAL MODEL AND STUDY PARTICIPANT DETAILS

Cell culture

ES-E14TG2a (E14) embryonic stem cells from male *Mus musculus* origin (RRID:CVCL9108[108]) were grown at 37°C and 5% CO_2 in DMEM base medium supplemented with 10% FBS, 1X nonessential amino acids, 2mM L-glutamine, β-mercaptoethanol and LIF on 10-cm plates precoated with 0.2% gelatin. Cells were passaged every ~48 h using trypsin and split at a ratio of ~1:8 with fresh medium. Routine anti-mycoplasma TC hood cleaning was conducted (LookOut DNA Erase spray) and cell lines were screened to confirm no mycoplasma presence. Cell lines are authenticated through sequencing.

METHOD DETAILS

Cell line generation

Chd4-dTAG-3XV5, Hltf-dTAG-3XV5, and Chd8-dTAG-3XV5 cell lines were made using CRISPR/Cas9-directed homologous recombination. Low passage wildtype ES cells were transfected with sgRNAs, a homology construct, and FuGene HD (Promega E2311) to generate endogenously tagged depletion cell lines. sgRNAs were designed using CRISPICK, cloned into the px330 plasmid containing a puromycin resistance cassette (Table S4). Homology constructs with $FKBP12^{F36V}$ and 3XV5 were purchased from ThermoFisher as GeneArt (Table S4). Genomic DNA from targeted cell lines were screened using PCR genotyping. Homozygous cell lines were verified by Sanger sequencing and western blotting for V5. Depletion was verified by western blotting. Experiments

were performed with two independently generated clones for Chd4-dTAG and Chd8-dTAG and technical replicate of one clone for Hltf-dTAG.

esiRNA generation

Endoribonuclease-digested short interfering RNAs (esiRNAs) were generated as previously described.[16,128] esiRNAs for all genes targeted in this study were designed and produced using the following protocol. Sequences for esiRNA design were selected by downloading and identifying common exons shared by all confirmed transcript isoforms of each remodeler ATPase according to NCBI. Next, these regions were used as input into DEQOR[110] and regions predicted to have no off-targets and high likelihood of knockdown efficiency were selected (Table S4). Using the identified regions, oligos were designed containing the T7 promoter sequence (Table S4). Next, the following primary PCR reaction was assembled in 200 μL tubes: 14 μL of nuclease-free water, 0.5 μL of 10 μM target specific forward primer, 0.5 μL of 10 μM target specific reverse primer, 0.5 μL of 10 mM dNTPs, 2 μL of 10X Thermo PCR buffer (NEB), 2 μL of ES-E14 wildtype cDNA template or from 1 μL plasmid pLJM1-EGFP for GFP esiRNAs, and 0.5 μL of Taq Polymerase (NEB), and the following PCR reaction was performed: 1) 94°C for 5 min, 2) 94°C for 30 s, 3) 65°C for 30 s, 4) 72°C for 2 min, repeating steps 2–4 for 35 total cycles, then 72°C for 2 min. The primary PCR product was diluted 1:200 in nuclease-free water and used as a template for the secondary PCR reaction as follows: 40.5 μL of nuclease free water, 5 μL of 10X Thermo PCR buffer, 1 μL of 10 mM dNTPs, 2 μL of 10 mM T7 primer, 0.5 μL of Taq Polymerase, 1 μL of 1:200 primary PCR product. Secondary PCR reactions were amplified using the following parameters: 1) 94°C for 2 min, 2) 94°C for 30 s, 3) 42° for 45 s, 4) 72°C for 1 min, repeating steps 2–4 for 5 total cycles, 5) 94°C for 30 s, 6) 60°C for 45 s, and 7) 72°C for 1 min, repeating steps 5–7 for 30 total cycles, then 7) 72°C for 5 min. Secondary PCR reactions were combined, ethanol/salt precipitated, and resuspended in 50 μL nuclease-free water. Combined and precipitated secondary PCR product was then used as template for the following *in vitro* transcription (IVT) reaction: 9 μL of combined and precipitated secondary PCR product, 6 μL of 25 mM NTPs, 4 μL of 5X T7 buffer (0.4 M HEPES pH 7.6, 0.2 M DTT, 120 mM $MgCl_2$, 10 mM Spermidine), and 1 μL of T7 Polymerase. The IVT reactions were incubated in a thermocycler using the following program: 1) 37°C for 5 h 30 min, 2) 90°C for 3 min, 3) ramp down (0.1 °C/s) to 70°C, 4) 70°C for 3 min, 5) ramp down (0.1 °C/s) to 50°C, 6) 50°C for 3 min, 7) ramp down (0.1 °C/s) to 25°C, and then 8) 25°C for 3 min. Next, IVT products were treated with 1 U of DNase I (NEB) at 37°C for 15 min and brought to a final volume of 100 μL with nuclease-free water. Finally, IVT products were digested with Shortcut RNase III (NEB) and purified using the PureLink RNA Mini Kit (Invitrogen) according to the following modified protocol: 200 μL of Lysis buffer (from RNA Mini Kit) was added to the IVT products, vortexed for 10 s, then 260 μL of 100% isopropanol was added and vortexed for an additional 15 s. Samples were then applied to a supplied spin column (from RNA Mini Kit), centrifuged for 30 s at 10,000 rcf, and the flowthrough was transferred to a new 1.5 mL tube, discarding the column. 700 μL of 100% isopropanol was added to the flowthrough, and vortexed for 15 s. 700 μL of the sample was applied to a new spin column, centrifuged for 30 s at 10,000 rcf, and the flowthrough was discarded. This process was repeated until the entire sample was applied to the column. 500 μL of Wash buffer 2 (from RNA Mini Kit) was added to the column, which was centrifuged for 30 s at 10,000 rcf. Then, 30 μL of nuclease-free water was applied to column, and samples were incubated for 1 min at room temperature, then centrifuged for 30 s at 10,000 rcf. This process was repeated a second time for a total eluent volume of 60 μL. Final esiRNAs were quantified using a Nanodrop and visualized on a 1.5% agarose gel to assure no undigested product remained.

esiRNA transfection

Reverse transfections were performed using 3500–5000 ng of either target or control (GFP) esiRNAs, 25 μL of Lipofectamine 3000, and 2 mL of OptiMEM media, incubated for 15–30 min at room temperature (RT). During this incubation, ES cells were counted and diluted to 350,000 cells/mL in ES cell media. After incubation, the transfection reaction was added to 4 mL diluted cell suspension and transferred to a pre-gelatinized 10 cm plate. After 16–18 h, the media was replaced with 6 mL fresh ES cell media. Cells were either treated with 4sU or harvested 48 h post-transfection for downstream assays, described below.

RT-qPCR

RNA isolated from transfected cells was quantified using a Nanodrop, and 1 μg of RNA was mixed with 2 μL of 10 mM dNTP mixture, 1 μL of random hexamers (Promega), and brought to 20 μL total volume with nuclease-free water. Samples were then incubated in a thermocycler at 68°C for 5 min, then placed on ice for 2 min. Then, 8 μL of First Strand buffer (Invitrogen), 4 μL of 0.1M DTT, 7 μL of nuclease-free water, and 1 μL of homemade reverse transcriptase (RT) were added to each sample, mixed by pipetting, and samples were placed into a thermocycler. The following program was used: 42°C for 90 min and 70°C for 15 min. For each sample, three technical replicates of 1 μL cDNA, 5 μL 2x SYBR GREEN, 2 μL nuclease-free water, and 1 μL 5 mM sample-specific forward and reverse qPCR primers (Table S4) were combined and run on a Roche Light Cycler for 25 cycles. Abundance of the target transcript in depleted samples was determined using the ΔΔCT normalization method relative to control samples, using *Gapdh* transcript abundance for internal normalization as previously described.[129]

Western blotting

Protein extracts were prepared using RIPA as previously described.[130] For remodeler depletion, 50 μg of protein was diluted in diluted in SDS loading buffer, run on 8% SDS-polyacrylamide gels for 2 h at 120V and transferred overnight to nitrocellulose membranes at 20V. Loading was measured with REVERT 700 total protein stain (LICORbio, 926–11011) and imaged by LI-COR (LI-COR

Odyssey DLx Imager). Antibodies were: CHD1 (Diagenode C15410334, 1:2000 in 1X PBST +5% BSA), CHD4 (abcam ab70469, 1:1000 in 1X PBST), CHD8 NOVUS nb10060418, 1:2000 in 1X PBST), BRG1 (Bethyl A300-813A, 1:1000 in 1X PBST), BTAF1 (abcam ab72285, 1:1000 in 1X PBST), SMARCAL1 (Santa Cruz SC-376377, 1:500 in 1X PBST), CHD2 (Invitrogen MA5-47275, 1:500 in 1X PBST), INO80 (Invitrogen PA5-65296, 1:1000 in 1X PBST), SNF2H (Invitrogen PA5-52601, 1:1000 in 1X PBST), SMARCAD1 (Invitrogen PA5-53482, 1:2000 in 1X PBST), and V5 (for CHD4-, CHD8-, and HLTF-dTAG proteins; Invitrogen R960-25, 1:1000 in 1XPBST). After overnight incubation with primary antibodies and washing, fluorescent conjugated 800nm secondary antibody (1:10,000 in 1XPBST) were added for 1 h in the dark and membanes were imaged by LI-COR.

For chromatin salt fractionation, 10 μL of each fraction was loaded on 10% SDS-polyacrylamide gels for 2 h at 120V and transferred overnight to nitrocellulose membranes at 20V. Loading was measured with REVERT 700 total protein stain (LICORbio, 926–11011) and imaged by LI-COR (LI-COR Odyssey DLx Imager). Tubulin (Sigma T6793, 1:5,000 in 1XPBST) was used as a cytosolic control, H3 (abcam ab1791, 1:1,000 in 1XPBST) was used as a nuclear marker, and remodelers (SMARCAL1 (Santa Cruz SC-376377, 1:500 in 1X PBST), CHD8 (NOVUS nb10060418, 1:2000 in 1X PBST), and SRCAP (Kerafast ESL103, 1:1,000 in 1XPBST) were assessed.

Transient Transcriptome sequencing (TT-seq)

TT-seq was conducted as previously described.[130,131] 48 h post transfection, media was aspirated from transfected plates and replaced with 10 mL of 500 nM 4-thio-uridine (4sU) containing ESC media and the plates incubated at 37°C with 5% CO_2 for 5 min. After 5 min, the 4sU-containing media was aspirated and the cells were washed with PBS, typsinized, and then pelleted by centrifugation. Total RNA was collected from cell pellets with a TRIzol extraction followed by an isopropanol/salt precipitation and resuspended in 100 μL 1XTE, according to ThermoFisher's recommendations. RNA concentration was determined by Qubit with the Qubit RNA broad range quantification kit (ThermoFisher). 1 μg of RNA was used as a template for RT-qPCR to determine esiRNA depletion efficiency, as described above. 100 μg of total RNA was diluted to a concentration of 240 ng/μL at a volume of 416.67 μL in 1XTE and then fragmented with a Bioruptor Pico (Diagenode) on high power for one 30 s cycle. The fragmented RNA was then combined with 283.33 μL 1XTE, 100 μL 10X Biotinylation buffer (100 mM Tris pH 7.4 and 10 mM EDTA), and 200 μL of 1 mg/mL biotin-HPDP (ThermoFisher) in dimethylformamide (DMF; freshly prepared). Samples were vortexed, then incubated in a thermomixer at 37°C shaking at 1000 RPM in the dark for 2 h. Samples were then chloroform extracted, isopropanol/salt precipitated, and resuspended in 22 μL of nuclease-free water. Streptavidin C1 beads (Invitrogen) were prepared for RNA separation as follows: 60 μL of beads were rotated for 2 min at room temperature RT with 1 mL of 1 M NaOH and 50 mM NaCl and then placed in the magnetic rack for 1 min. The supernatant was discarded, and beads were resuspended in 1 mL of 100 mM NaCl. Beads were washed twice with 1 mL of 100 mM NaCl and resuspended in 60 μL of TT-seq Binding buffer (10 nM Tris pH 7.4, 300 mM NaCl, 0.1% Triton). Then, 60 μL of prepared streptavidin C1 beads were added to each sample and rotated at room temperature for 20 min. Following incubation, the samples were magnetized for 1 min and the supernatant (containing the unlabeled RNA) was placed in a separate 1.5 mL tube and put on ice. The unlabeled RNA from supernatant was PCI/chloroform extracted, isopropanol/salt precipitated, and resuspended in 100 μL of nuclease-free water. The bead-bound labeled nascent RNA was washed twice with 500 μL of High Salt buffer (50 mM Tris pH 7.4, 2 M NaCl, 0.5% Triton), twice with 500 μL of TT-seq Binding buffer, and once with 500 μL of Low Salt buffer (5 mM Tris pH 7.4, 0.1% Triton), rotating for 1 min at RT, re-magnetizing and resuspending the beads during each wash. The nascent RNA was eluted by resuspending beads in 100 μL of freshly prepared 100 mM DTT and incubating in a thermomixer at 65°C and 1000 RPM shaking for 5 min. The beads were magnetized and the supernatant was transferred to a new tube, and a second elution from the beads was performed. Eluted nascent RNA were pooled and the nascent RNA was recovered with a PCI extraction and an isopropanol/salt/glycogen precipitation. RNA pellets were resuspended in 25 μL of nuclease-free water. The total RNA and nascent RNA from each sample were used to build RNA-seq and TT-seq libraries, respectively, as described below.

RNA-seq library preparation

RNA-seq libraries were built using a custom strand-specific RNA-seq library build protocol that includes an antisense oligo (ASO)-based rRNA depletion protocol. First, 2 μg of total RNA was combined with 2 μL of 0.5 μM pooled antisense rRNA oligos (at a ratio of 1 μL of 0.5 μM pooled antisense rRNA oligos per μg total RNA) and rRNA hybridization buffer (100 mM Tris-Cl pH 7.4, 200 mM NaCl) to a final volume of 10 μL. In a thermocycler, the samples were heated at 95°C for 5 min, then slowly cooled down to 22 °C at a rate of −0.1 °C/s, followed by incubation at 22°C for 5 min, then placed on ice. Next, 2 μL of thermostable RNase H (10 units; Epicentre), 2 μL of 10X RNase H buffer (Epicentre) and 6 μL of nuclease-free water were added and the samples were incubated at 45°C for 30 min. Then, 2 μL of Turbo DNase (ThermoFisher) and 5 μL of 10X Turbo DNase buffer (ThermoFisher) were added and samples were incubated at 37°C for 20 min. Samples were then purified using an RNA clean and concentrator kit (Zymo Research), according to the following protocol. Adjusted RNA Binding buffer was made by combining 50 μL of RNA Binding buffer with 50 μL of 100% ethanol and mixing well by pipetting or vortexing. Then, 100 μL of adjusted RNA Binding buffer was added to each sample and mixed well by vortexing, and then each sample was applied to a spin column supplied in the RNA clean and concentrator kit (Zymo Research). Samples were centrifuged at 12,500 rcf for 30 s, and the flowthrough was discarded. 400 μL of RNA Prep buffer was added and samples were centrifuged at 12,500 rcf for 30 s, and the flowthrough was discarded. 700 μL of RNA Wash buffer was added and samples were centrifuged at 12,500 rcf for 30 s, and the flowthrough was discarded. 400 μL of RNA Wash buffer was added and samples were centrifuged at 12,500 rcf for 2 min, and flowthrough was discarded. Samples were centrifuged again at 12,500 rcf for 1 min to remove any residual RNA Wash buffer, and the columns were transferred to fresh 1.5 mL microfuge tubes. 11 μL of nuclease-free water was

added to each column and incubated for 1 min at room temperature before spinning at 12,500 rcf for 1 min. Samples were transferred to 200 μL tubes, 5 μL 5X First Strand buffer (Invitrogen) was added, and the samples were heated at 95°C for 5 min in a thermocycler. Then, 1 μL of 6 M random hexamers were added to each sample and incubated at 65°C for 3 min. Next, 5.25 μL of nuclease-free water, 1.5 μL of 10 mM dNTPs, 1.25 μL of 100 mM DTT, and 1 μL of Superscript III (Invitrogen) were added to each sample, and then placed in a thermocycler with the following program: 25°C for 5 min, 50°C for 1 h, and 70°C for 15 min. Next, samples were purified using 45 μL AMPure XP beads (Beckman Coulter) according to the manufacturer's instructions and eluted in 22 μL of 0.1X TE. 20 μL of eluted sample was transferred to fresh 200 μL tubes. To each sample, 3 μL of 10X NEB buffer 2, 2 μL of dUTP mixture (20 mM dUTP, 10 mM dATP, 10 mM dCTP, 10 mM dGTP), 0.5 μL of 100 mM DTT, 1 μL of RNase H (Epicentre), and 2 μL of DNA Polymerase I (10U/μL, NEB) were added and mixed by pipetting, then the samples were incubated in a thermocycler at 16°C for 2.5 h. Samples were then purified with 45 μL AMPure XP beads (Beckman Coulter) according to the manufacturer's instructions and eluted with 32 μL 0.1X TE. 30 μL of eluted sample was transferred to fresh 200 μL tubes. To each sample, 3 μL of nuclease-free water, 5 μL of 10X T4 DNA Ligase buffer (with 10mM ATP), 5 μL of 10 mM dNTP mix, 2 μL of T4 DNA Polymerase (3 U/μL, NEB) 1 μL of Klenow DNA Polymerase (5 U/μL, NEB) and 2 μL of T4 PNK (10 U/μL, NEB) were added, and the samples were incubated in a thermocycler at 20°C for 30 min. Next, 35 μL of AMPure XP beads were added to each sample and mixed by vortex, and incubated at RT for 5 min, then magnetized on a magnetic rack for 3 min. The supernatant was transferred to new 200 μL tubes, and then the samples were purified with 102 μL AMPure XP beads according to the manufacturer's instructions and eluted with 22 μL 0.1XTE and 20 μL of eluted sample was transferred to fresh 200 μL tubes. To each sample, 9 μL of nuclease-free water, 5 μL of NEB buffer 2, 1 μL of 10 mM dATP, and 3 μL of Klenow 3′ to 5′ exo (5 U/μL, NEB), and samples were incubated in a thermocycler at 37°C for 30 min. This was followed with a purification with 60 μL AMPure XP beads according to the manufacturer's instructions, eluted with 22 μL 0.1XTE and transferred to fresh 200 μL tubes. For adapter ligation, NEBNext adapters were thawed on ice and diluted 1:5 in nuclease-free water to final concentration of 5 mM, and then 25 μL of 2X Quick Ligase buffer, 1 μL 10 mM NEBNext adapter, 2 μL of T4 DNA ligase (NEB) were added and incubated at RT for 30 min 3 μL USER enzyme (NEB) were added to each sample and incubated at 37°C for 15 min and followed by a purification with 50 μL AMPure XP beads according to the manufacturer's instructions, eluted with 30 μL 0.1XTE and transferred to fresh 200 μL tubes. To each sample, 1 μL of 10 μM NEBNext i7 Primer (Universal), 1 μL of 10 μM NEBNext i5 Primer, 10 μL nuclease-free water, 12 μL of 5X HF Phusion buffer, 2 μL of 10mM dNTPs mixture, and 1 μL of Phusion Polymerase (2 U/μL, NEB) were added and mixed by pipette. Samples were then placed in a thermocycler and the following PCR program was used: 1) 98°C for 30 s, 2) 98°C for 10 s, 3) 65°C for 30 s, 4) 72°C for 30 s, repeat steps 2–4 for a total of 10 cycles, and then 72°C for 3 min. A final bead cleanup was performed with 54 μL AMPure XP beads according to the manufacturer's instructions, eluted with 22 μL of 0.1XTE, and 20 μL of elutant was transferred to fresh 1.5 mL microfuge tubes. Libraries were quantified by Qubit with the dsDNA High Sensitivity Kit (ThermoFisher) and run on a Fragment Analyzer to confirm high quality of each library prior to sequencing. Libraries were paired-end sequenced on the Illumina NextSeq 500 platform with standard protocols at the UPMC Children's Hospital of Pittsburgh to a depth of ~40,000,000 uniquely mapped reads per sample.

TT-seq library preparation

TT-seq libraries were built using the NEBNext Ultra II RNA Library prep kit for Illumina (NEB) according to the manufacturer's recommendations, with specific modifications as described below. 100 ng of nascent RNA was rRNA depleted using antisense oligo rRNA depletion as described for RNA-seq libraries, but with 0.05 μM pooled antisense rRNA oligos to account for the adjusted amount of input material. To account for using rRNA-depleted nascent RNA as input for the library build, we adjusted the volumes of the Fragmentation and Priming mix, First Strand Synthesis Reaction, and Second Strand Synthesis Reaction as follows: Fragmentation and Priming mix: 10 μL of rRNA-Depleted nascent RNA, 8 μL of NEBNext First Strand Synthesis Reaction buffer, 2 μL of Random Primers; First Strand Synthesis Reaction: 20 μL of RNA, 16 μL of NEBNext Strand Specificity Reagent, and 4 μL of NEBNext First Strand Synthesis Enzyme Mix; Second Strand Synthesis Reaction: 40 μL of First Strand Synthesis product, 8 μL of NEBNext Second Strand Synthesis Reaction buffer with 10X dUTP Mix, 4 μL NEBNext Second Strand Synthesis Enzyme Mix, and 28 μL nuclease-free water. RNA was fragmented for 15 min, NEBNext Adaptor and primers were diluted 1:5, and 7 PCR amplification cycles were performed for all TT-seq library builds. Libraries were quantified by Qubit with the dsDNA High Sensitivity kit and run on a Fragment Analyzer to confirm high quality of each library prior to sequencing. TT-seq libraries were paired-end sequenced on the Illumina NextSeq 500 platform with standard protocols at the UPMC Children's Hospital of Pittsburgh to a depth of ~40,000,000 uniquely mapped reads per sample.

CUT&RUN

CUT&RUN experiments were performed as previously described,[130,132,133] with the following modifications. The following antibodies were used in CUT&RUN experiments performed on 100,000 lightly crosslinked wildtype ES cells using a low salt elution method for fragment release: SRCAP (Kerafast ESL103,1:50) SMARCAL1 (Invitrogen PA5-28980, lot YF3945097B, 1:50), and IgG (Sigma-Aldrich, 06–371,1:250). The following antibodies were used in low salt elution uncrosslinked CUT&RUN experiments on 100,000 cells transfected by esiRNAs: H3K27ac (abcam ab4729, lot GR3416784-1, 1:100), H2A.Z (abcam ab4174, lot GR3198864-1, 1:100), NFYA (Santa Cruz SC-17753, lot D2522, 1:50), SRCAP (Kerafast ESL103,1:50) SMARCAL1 (Invitrogen PA5-28980, lot YF3945097B, 1:50), CHD8 (NOVUS NB100-60418 lot A4), and IgG (Sigma-Aldrich, 06–371,1:250).

For lightly crosslinked wildtype ES cells: cells were washed with 1X PBS, typsinized, counted, and 1 million cells were collected in 1.5 mL microfuge tubes and placed on ice. Cells were centrifuged at 600 rcf at 4°C for 5 min, and the supernatant was removed without disturbing the pellet. The cell pellet was resuspended gently in 1 mL ESC media +0.1% formaldehyde, inverted 3 times, and crosslinked for 5 min at RT. The reaction was then quenched with 100 μL of 2.5M glycine. For 48-h post esiRNA transfected cells: cells were washed with 1X PBS, typsinized, counted, and 600,000 cells were collected in 1.5 mL microfuge tubes and placed on ice. Cells were centrifuged at 600 rcf at 4°C for 5 min, and the supernatant was removed without disturbing the pellet. The cell pellet was resuspended gently in 1 mL cold 1X PBS and centrifuged at 600 rcf at 4°C for 5 min, and the supernatant was removed without disturbing the cell pellet. The cells were then gently resuspended in 1 mL cold Nuclear Extraction (NE) buffer (20 mM HEPES-KOH, pH 7.9, 10 mM KCl, 0.5mM spermidine, 0.1% Triton X-100, 20% glycerol, freshly added protease inhibitors) and incubated on ice for 10 min. After incubation, the lysed cells were centrifuged at 600 rcf at 4°C for 5 min, and the supernatant was removed without disturbing the nuclei pellet, and the pellet was flash frozen. Prior to experimentation, pellets were thawed on ice for 5 min and resuspended in 600 μL cold NE buffer.

To prepare lectin-coated concanavalin beads (Polysciences), 25 μL of beads per 100,000 nuclei in each aliquot were combined with 850 μL Binding buffer (20 mM HEPES, pH 7.5, 150 mM NaCl, 0.5 mM spermidine, 0.1% BSA, 2 mM EDTA, fresh protease inhibitors) in a fresh tube, washed twice with 1 mL Binding buffer on a magnetic rack, and resuspended in 300 μL Binding buffer. While gently vortexing the nuclei, 300 μL of bead slurry was slowly added to the cell nuclei and reaction was rotated at 4°C for 10 min. Next, the samples were placed on a magnetic rack until the solution cleared (~5 min), and the supernatant was removed without disturbing the beads. The beads were resuspended in 1 mL Blocking buffer (20 mM HEPES, pH 7.5, 150 mM NaCl, 0.5 mM spermidine, 0.1% BSA, 2mM EDTA, freshly added protease inhibitors) with gentle pipetting, and then incubated at RT for 5 min. The samples were then placed on the magnet stand, the supernatant was removed and then gently resuspended in 1 mL Wash buffer (20 mM HEPES, pH 7.5, 150 mM NaCl, 0.5 mM spermidine, 0.1% BSA, freshly added protease inhibitors). The samples were placed on a magnetic stand, the supernatant was removed, and resuspended in 125 μL Wash buffer per 100,000 nuclei aliquot and divided into individual 100,000 nuclei aliquots. Next, primary antibody mix (125 μL Wash buffer with target specific antibody at specified dilutions) was added to each sample while gently pipetting and then incubated on a rotator for 1 h at 4°C for lightly crosslinked nuclei or at RT for transfected nuclei. Samples were placed on a magnetic rack, allowed to clear and the supernatant was removed and discarded. Samples were washed twice with 1 mL Wash buffer, resuspending each time by pipetting. After washing, the samples were resuspended in 125 μL Wash buffer, and 125 μL pA-MNase (for rabbit antibodies) or pAG-MNase (for mouse antibodies) mix was added to each sample while gently vortexing. Samples were then rotated for 30 min at 4°C for lightly crosslinked nuclei or at RT for transfected nuclei. Samples were washed twice with 1 mL Wash buffer as above, resuspended in 150 μL Wash buffer and placed in an ice/water bath for 5 min to cool to 0°C. After incubation, 3 μL of 100 mM $CaCl_2$ was added to each sample by gently vortexing and flicking 2–3 times to mix well and placed back into the ice bath for 1 h for crosslinked nuclei or 30 min for transfected nuclei. After 1 h or 30 min exactly as indicated, 150 μL of 2xSTOP buffer (200 mM NaCl, 20 mM EDTA, 4 mM EGTA, 1% NP40, 0.2 mg/mL glycogen, and 0.05 ng/mL *S. cerevisiae* DNA spike-in) was added to each sample and mixed by pipetting. Samples were then incubated at 4°C for 1 h to facilitate low-salt fragment release from bead-bound nuclei. Next, samples were placed onto the magnetic rack, and the supernatant was transferred to fresh 1.5 mL microfuge tube without disturbing the beads. Next, 20 μL 5M NaCl and 1.5 μL RNase A (Invitrogen) was added to each sample, mixed well by pipette, then incubated at 37°C for 20 min in a thermomixer. Then, 2.5 μL of Proteinase K and 3 μL of 10% SDS was added, mixed by quick vortex, and then incubated for 10 min at 70°C. At this stage, lightly crosslinked nuclei were then incubated at 55°C overnight to reverse crosslinking. Next, 300 μL of PCI was added to each sample and vortexed for 15 s on highest setting. The samples were then transferred to phase lock tubes and centrifuged for 5 min at 4 °C at 16,000 rcf. Then, 300 μL of chloroform was added to each sample and vortexed for 15 s on the highest setting. The samples were centrifuged for 5 min at 4 °C at 16,000 rcf, the aqueous fraction was transferred to a new 1.5 mL microfuge tube. For lightly crosslinked samples, 150 μL of AMPure XP beads were added to the aqueous fraction, mixed well by vortex, and incubated for 15 min at RT. Samples were then magnetized for 5 min at RT, and the supernatant was transferred to a new tube, and 1 mL of 100% ethanol and 5 μL of 20 mg/mL glycogen was added and vortexed for 15 s on the highest setting. For transfected nuclei (not crosslinked), the aqueous fraction was transferred to a new tube, and 750 μL of 100% ethanol and 5 μL of 20 mg/mL glycogen were added and vortexed for 15 s on the highest setting. The samples were incubated for 30 min at −20°C, and then centrifuged at 16,000 rcf for 30 min at 4°C. The supernatant was discarded, and the DNA pellet was washed with 1 mL of 80% ethanol. Next, the samples were centrifuged at 16,000 rcf for 5 min at 4°C and the supernatant was discarded. Pellets were allowed to air dry for approximately 5 min and resuspended in 50 μL of 0.1XTE.

CUT&RUN library build

On ice in 200 μL tubes, 7 μL of NEBNext Ultra II End Prep Enzyme buffer (NEB) and 3 μL of NEBNext Ultra II End Prep Enzyme Mix (NEB) were added to each sample and mixed well by pipetting up and down. Samples were placed in a thermocycler with the following program: 20°C for 30 min, then 65°C for 30 min. Next, 5 μL of 1.5 μM NEB adapter, 5 μL of T4 DNA ligase, and 55 μL of 2X Quick Ligase buffer were added to each sample and then mixed by pipetting. Samples were incubated in a thermocycler at 20°C for 15 min, then 3 μL of USER enzyme (NEB) was added and mixed again by pipetting. Samples were incubated in a thermocycler at 37°C for 15 min, then purified with 128 μL of AMPure XP beads (Beckman Coulter) according to the manufacturer's instructions and eluted in 30 μL of 0.1X TE buffer. After elution, 27.5 μL of each sample were transferred to fresh 200 μL tubes. To each sample, 10 μL of 5X KAPA HF buffer, 1 μL of KAPA HIFI polymerase, 1.5 μL of 10 mM dNTP mix, 5 μL of 1.5 μM NEBNext i5 Universal PCR

primer, and 5 μL of 1.5 μM NEBNext i7 PCR primer were added and mixed well by pipetting. Samples were then placed in a thermocycler and then PCR amplified using the following program: 1) 98°C for 45 s, 2) 98°C for 15 s, 3) 60°C for 10 s, repeat steps 2–3 for 15 total cycles, and 4) 72°C for 1 min. Samples were then purified with 60 μL of AMPure XP beads according to the manufacturer's instructions, eluted in 30 μL of 0.1X TE buffer, and 27.5 μL of amplified library were transferred to fresh tubes. A fraction of each library was run on a 1.5% agarose gel and quantified by Qubit High Sensitivity dsDNA quantification kit to ensure high quality. CUT&RUN libraries were paired-end sequenced on the Illumina NextSeq500 platform with standard protocols at the UPMC Children's Hospital of Pittsburgh to a depth of ~10,000,000 uniquely mapped reads per sample.

Chromatin salt fractionation

Cells were transfected with esiRNAs target control (GFP), *Srcap*, *Chd8*, or *Smarcal1* as described above. At 48 h post-transfection, the cells were washed with 1X PBS, typsinized, counted, and 10 million cells were collected in a 1.5 mL microfuge tube and placed on ice. Cells were resuspended in 1 mL of hypotonic buffer (10 mM HEPES, pH 7.9, 1.5 mM $MgCl_2$, 10 mM KCl, 0.5 mM DTT, protease inhibitors) and incubated on ice for 30 min. Cell suspension was transferred to a pre-cooled Dounce homogenizer and cell membrane as disrupted using 40 strokes with a tight-fitting pestle. Cells were centrifuged at 1,500 rcf for 5 min at 4°C and the supernatant was collected as and held on ice as the cytosolic fraction. Nuclei were resuspended in 400 μL Buffer III.A (10mM Tris pH 7.4, 2mM $MgCl_2$, 5mM $CaCl_2$, protease inhibitors) by pipetting and digested with 5 U MNase at 37°C for 30 min. The reaction was quenched with 25 μL 0.1 M EGTA and an aliquot was saved as the nuclear fraction. Sample was centrifuged at 400 rcf for 10 min at 4°C and the chromatin pellet was resuspended in 400uL Buffer III.B (10 mM Tris pH 7.4, 2 mM $MgCl_2$, protease inhibitors). Sample was centrifuged at 400 rcf for 10 min at 4°C and the supernatant was discarded. To sequentially elute more tightly bound protein using increasing amounts of salt, nuclei were resuspened in 400 μL Buffer IV (10 mM Tris pH 7.4, 2 mM $MgCl_2$, 2 mM EGTA, 0.1% Triton X-100) with NaCl concentrations ranging from 80 mM to 600 mM. During each fraction, samples were incubated at 4C with rotation for 30 min, and centrifuged at 400 rcf for 10 min at 4°C to collected the fraction. Samples were prepared immediately for western blot.

ATAC-seq

Cells were transfected with esiRNAs as described above. At 48 h post-transfection, the cells were washed with 1X PBS, typsinized, counted, and 50,000 cells were collected in a 1.5 mL microfuge tube and placed on ice. Cells were centrifuged at 600 rcf at 4°C for 5 min, and the supernatant was removed without disturbing the pellet. The cell pellet was resuspended gently in 1 mL cold 1X PBS, centrifuged at 600 rcf at 4°C for 5 min, and the supernatant was removed without disturbing the cell pellet. The cells were then gently resuspended in 600 μL of cold NE buffer (20 mM HEPES-KOH, pH 7.9, 10 mM KCl, 0.5mM spermidine, 0.1% Triton X-100, 20% glycerol, freshly added protease inhibitors) and incubated on ice for 10 min. After incubation, the samples were centrifuged at 600 rcf at 4°C for 5 min, and the supernatant was removed without disturbing the nuclei pellet. Pellets were flash frozen and stored in the −80°C until use. Prior to use, nuclei were thawed on ice (~5 min). Nuclei were gently resuspended in 50 μL of Transposase mix (25 μL Transposase buffer, 16.5 μL 1X PBS, 0.5 μL 10% Tween 20, 0.5 μL 1% digitonin, 5 μL nuclease-free water, 2 μL Tagmentase (Diagenode), and then incubated at 37°C for 30 min with 1000 rpm on a thermomixer. After incubation, the samples were isolated using a DNA Clean and Concentrator Kit (Zymo Research) according to the manufacturer's instructions and eluted in 10 μL of DNA elution buffer.

ATAC-seq library preparation

To 10 μL of eluted sample in 200 μL tubes, 2.5 μL 25 μM Nextera i7 primer, 2.5 μL 25 μM Nextera i5 primer, 10 μL nuclease-free water, and 25 μL Nextera High Fidelity 2X PCR Master Mix were added and mixed by pipetting. Samples were then PCR amplified using the following program: 1) 72°C for 5 min, 2) 98°C for 30 s, 3) 98°C for 10 s 4) 63°C 30 s, repeat steps 3–4 for 5 total cycles, and 5) 72°C for 1 min. Samples were placed on ice and 1 μL of the partially amplified sample was added to 1 μL 2 μM Nextera primer 1, 1 μL 2 μM Nextera primer 2, 3 μL nuclease-free water, and 5 μL 2X SYBR green and mixed well by pipetting while avoiding air bubbles. qPCR was performed with the following program: 1) 72°C for 5 min, 2) 98°C for 30 s, 3) 98°C for 10 s 4) 63°C 30 s, repeat steps 3–4 for 20 total cycles, and 5) 72°C for 1 min, and the number of additional PCR cycles needed for each sample, by determining the number of cycles needed to reach 1/3 of the max R. Samples were then amplified for 8–9 total cycles as determined by qPCR. Amplified libraries were run on a 1.5% agarose gel and DNA fragments 150–500 base pairs were extracted and gel purified, and the final library concentration was determined by Qubit High Sensitivity dsDNA quantification kit. ATAC-seq libraries were paired-end sequenced on the Illumina NextSeq500 platform with standard protocols at the UPMC Children's Hospital of Pittsburgh to a depth of ~30,000,000 uniquely mapped reads per sample.

QUANTIFICATION AND STATISTICAL ANALYSIS

TT-seq and RNA-seq data analysis

Feature definitions

Protein coding RNAs were defined from protein coding genes using the mm10 Gencode genome annotation V23,[50] for a final dataset of 21,596 protein coding genes. uaRNA were defined as the antisense region −1500 base pairs upstream to +500 base pairs downstream of all protein coding transcript TSSs from protein coding genes in the mm10 GENCODE genome annotation. uaRNA regions overlapping with protein coding and long non-coding RNA genes and less than 5 kb downstream of any protein coding gene or

annotated long non-coding RNA were removed, and overlapping features were merged for a final dataset of 26,605 regions. Protein coding RNAs and uaRNAs were counted in a strand-specific manner. Enhancer regions were defined with previously described gene-distal DNase 1 hypersensitive sites (GSM1014154[134]), after removing all features within 1 kb of the TSSs annotated mm10 coding genes and those overlapping uaRNA regions. To each remaining DHS, 500 base pairs upstream and downstream were added and merging overlapping regions for a final dataset of 101,587 DHS regions. Enhancers overlapping protein coding genes were counted in a strand-specific manner on the antisense strand, while enhancers within intergenic were counted in an unstranded manner.

Paired-end fastq files were trimmed and adapters were removed with trimmomatic[111] and cutadapt.[112] Reads were aligned to the mm10 genome using STAR[113] with options –outSAMtype SAM, –outFilterMismatchNoverReadLmax 0.02, and –outFilterMultimapNmax 1, and quality filtered using SAMtools[135] view with options -q 7, -f 2, -bS. Counts were generated using featurecounts,[115] with options -B -t "exon" -g "gene_name" -F GTF -p -s 2 for Gencode features, with options -B -F SAF -p -s 2 for non-coding features, using features as defined. Counts analyses were performed in the R/Bioconductor environment. Raw count matrices were corrected for batch effects using Combat-seq[116] as indicated in Table S6 with RNA-seq counts adjusted using all Gencode features, and TT-seq counts using all Gencode features and non-coding RNA features while using the experimental condition as the covariate. Differential gene expression analysis was performed using DEseq2[117] for all available replicates of each condition ($n = 2$ for experimental samples and $n = 17$ for control samples), only keeping features with at least 10 counts in 50% of samples and with option lfcShrink type = "apeglm". Differentially expressed mRNAs were defined as $|\log2(FC)| \geq 0.75$ and FDR$\leq$0.05 and differentially transcribed ncRNAs were defined as $|\log2(FC)| \geq 0.5$ and FDR$\leq$0.05. Gene Ontology analysis on gene sets of interest was performed the R package "clusterProfiler"[118] using all expressed mRNAs (TPM>0, TT-seq) as background. Strand specific bigwigs were generated with deepTools[119] using DEseq2-derived sizeFactors with binsize of 1, and averaged bigwigs were generated using all replicates for each condition. Differential bigwigs were generated in deepTools from averaged bigwigs. Browser track images were generated using IGV.[120]

Background signal analysis and cutoff thresholding

We included many control samples and therefore could confidently call noise vs. differentially expressed transcription units due to depletion using the thresholds we established (p.adj$\leq$0.05& $\log_2$FC $\geq$ 0.75 for mRNAs and p.adj$\leq$0.05& $\log_2$FC $\geq$ 0.5 for ncRNAs). To establish these thresholds, we performed an analysis where we used the control (GFP esiRNA) experiments, holding 2 as the experimental and 15 as the control (136 combinations in total). We did all 136 combinations of this analysis and found that adding together all the differentially transcribed (p.adj$\leq$0.05) mRNAs = 2491, uaRNAs = 44, eRNAs = 562, only an extremely small fraction are called as differential once our $\log_2$FC thresholds are applied: mRNAs = 22, uaRNAs = 8, and eRNAs = 116. Therefore, the cutoffs we selected robustly reduce background signal.

mRNA and uaRNA relationship analyses

For each condition, promoters showing significant mRNA and/or uaRNA transcriptional changes were sorted into one of four categories based on transcriptional changes: Only mRNA changes ($|\log_2$(mRNA change)$| \geq 0.75$, $|\log_2$(uaRNA change)$| < 0.5$), Only uaRNA changes ($|\log_2$(mRNA change)$| < 0.75$, $|\log_2$(uaRNA change)$| \geq 0.5$), Same directional changes ($\log_2$(mRNA change)$| \geq 0.75$, $|\log_2$(uaRNA change)$| \geq 0.5$ in same direction), or Opposite directional changes ($|\log_2$(mRNA change)$| \geq 0.75$, $|\log_2$(uaRNA change)$| \geq 0.5$ in opposite direction). For promoters in each category, directionality was calculated as the $\log_{10}$(mRNA counts/uaRNA counts). Statistical enrichment for promoters in each category was determined using as $p \leq 0.05$ with Chi-squared test for homogeneity assuming equal enrichment across all categories.

Predicted enhancer promoter pairing analysis

Enhancer promoter pairs (EPPs) were predicted in each condition by defining significantly changed promoters ($|\log_2(FC) \geq 0.75$ and FDR$\leq$0.05) and putative enhancers ($|\log_2(FC) \geq 0.5$ and FDR$\leq$0.05) changed in the same direction occurring within 100 kb, 250 kb, 500 kb, or 1Mb each other on the same chromosome using bedtools.[121]

We used an approach based on Heger et al. (2013)[136] to generate a distribution of expected EPPs per condition. For each condition, we used a custom script to perform 1000 permutations of randomly shuffling the start and end coordinates of each changed promoter and putative enhancer while preserving the element size and chromosome identity to control for differences in chromosome size, and predicted "expected" EPPs across 100 kb, 250 kb, 500 kb, and 1Mb distance thresholds. By randomizing both sets of genomic features of interest for each iteration, we also randomize gene density, which provides a robust readout for if the proximity of changed enhancers and promoters are truly random. With this approach, it is necessary to maintain the original sampling area size to keep the comparison with the observed data valid. p values for obtaining the observed number of predicted EPPs were calculated as: (sum of (number of tests with predicted EPPs $\geq$ observed number of EPPs))/number of tests and were adjusted using the Benjamini & Yekutieli approach. Enrichment was calculated as: the observed number of predicted EPPs/mean(expected number of EPPs).

ATAC-seq analysis

Paired end fastq files were processed using the PEPATAC[122] pipeline. Briefly, reads were trimmed using trimmomatic,[111] and aligned to the mm10 genome using bowtie2[123] with options –very-sensitive, -X 2000, and SAMtools[135] was used to remove reads

with MAPQ <10 and mitochondrial reads. Picard[125] was used to remove PCR duplicates. After alignment, we used the quality control metrics of the PEPATAC[122] pipeline to evaluate the quality of our ATAC-seq samples to ensure high sample quality. Next, SAMtools was used to merge all replicates of the control and experimental conditions, and then the merged files were then subsampled to the same read depth. Reads were corrected for Tn5 cutting bias by adding +4 bases for positive strand and −5 bases for negative strand using alignmentSieve in deepTools with –ATACshift. Next, peak calling on experimental and control samples was performed by MACS2[124] with –mode BAMPE –nomodel –shift 75. Using bedTools, peak files from the experimental and control samples were then merged, 50 base pairs on each side were added to each feature, and then overlapping features were again merged to generate a consensus peak set for each depletion condition. Peaks within the consensus peak set were further annotated as promoter or enhancer peaks if they occurred with 1 kb of these features. Overlaps with other peak sets were determined using bedtools.

Differential chromatin accessibility analysis

All available replicates were size class filtered for NFR size fragments (1–100 bp) using a custom script, and then all subsampled to the sample read depth using samtools. Reads were then corrected for Tn5 cutting bias using alignmentSieve –ATACshift in deepTools. Read counts on consensus peak sets for each condition were generated using bedtools coverage -counts, and count analyses were performed in R/Bioconductor environment. After removing all peaks with less than 10 counts in 50% of samples, differential accessibility analysis was performed using edgeR for all available replicates of each condition with RUVseq correction. Differentially accessible peaks were defined as $|\log_2(FC)| \geq 0.5$ and $FDR \leq 0.05$.

Tobias analysis

Replicate bam files were merged and subsampled using SAMtools to bring experimental and control merged bam files to the same read depth, and transcription factor foot printing analysis was performed using TOBIAS.[80] Transcription factor motifs were downloaded from the JASPAR[137] database, and TOBIAS ATACorrect and Score-BigWig were used to generate scored bigwig files across the consensus ATAC-seq peak dataset. TOBIAS BINDetect was used to determine differential binding scores for motifs in experimental and control conditions at promoters and putative enhancers. Only motifs of TFs with TPM $\geq$1 (RNA-seq) and $\geq$10 binding sites and p value $\leq$ 0.05 in both conditions at bound and unbound loci were considered.

CUT&RUN analysis

Paired end fastq files were trimmed to 25 bp and aligned to the mm10 genome using bowtie2 with options -I 10, -X 1000, -N 1, and –very-sensitive. Picard[125] was used to filter PCR duplicates. SAMtools was used to filter reads with MAPQ <10, and the reads were sorted into size classes according to the target (1–120 bp for all factors, and 150–500 bp for histone variants post-translational modifications). For peak calling, all replicate bams were merged, and MACS2 was used for peak calling against the corresponding IgG file using -f BAMPE and -q 0.001 for factors or –broad –broad-cut-off 0.001 for histone variants and modifications. All experimental and control peaks were merged to create a consensus peak set. Bedtools was used to define overlap between peak sets of interest. deepTools was used to generate bigwigs using RPGC normalization, –effectiveGenomeSize 2407883318, -e, -bs 5, and –smoothLength 20. deepTools was also used to generate differential bigwigs, heatmaps, and metaplots.

ChIP-seq analysis

The full list of all publicly available datasets used in this study can be found in Table S5 and the key resources table. Single end fastq files were trimmed using trimmomatic and aligned to the mm10 genome using bowtie2 with options –best –strata, and reads with MAPQ <10 were removed with SAMtools. For peak calling, all replicate bams were merged, and MACS2 was used for peak calling against the correspond input file using -q 0.001 and -f BAMPE for paired end files or -f BAM for single end files.

Differential peak enrichment analysis

CUT&RUN read counts on consensus peak sets for each condition were generated using bedtools coverage -counts, and count analyses were performed in R/Bioconductor environment. After removing all peaks with less than 10 counts in 50% of samples, differential accessibility analysis was performed using edgeR for all available replicates of each condition with RUVseq correction. Differentially enriched peaks were defined as $|\log_2(FC)| \geq 0.5$ and $FDR \leq 0.05$.

ADDITIONAL RESOURCES

No clinical trials were performed in this study.

Cell Reports, Volume *44*

Supplemental information

Widespread impact of nucleosome remodelers on transcription at *cis*-regulatory elements

Benjamin J. Patty, Rinku Dhungana, and Sarah J. Hainer

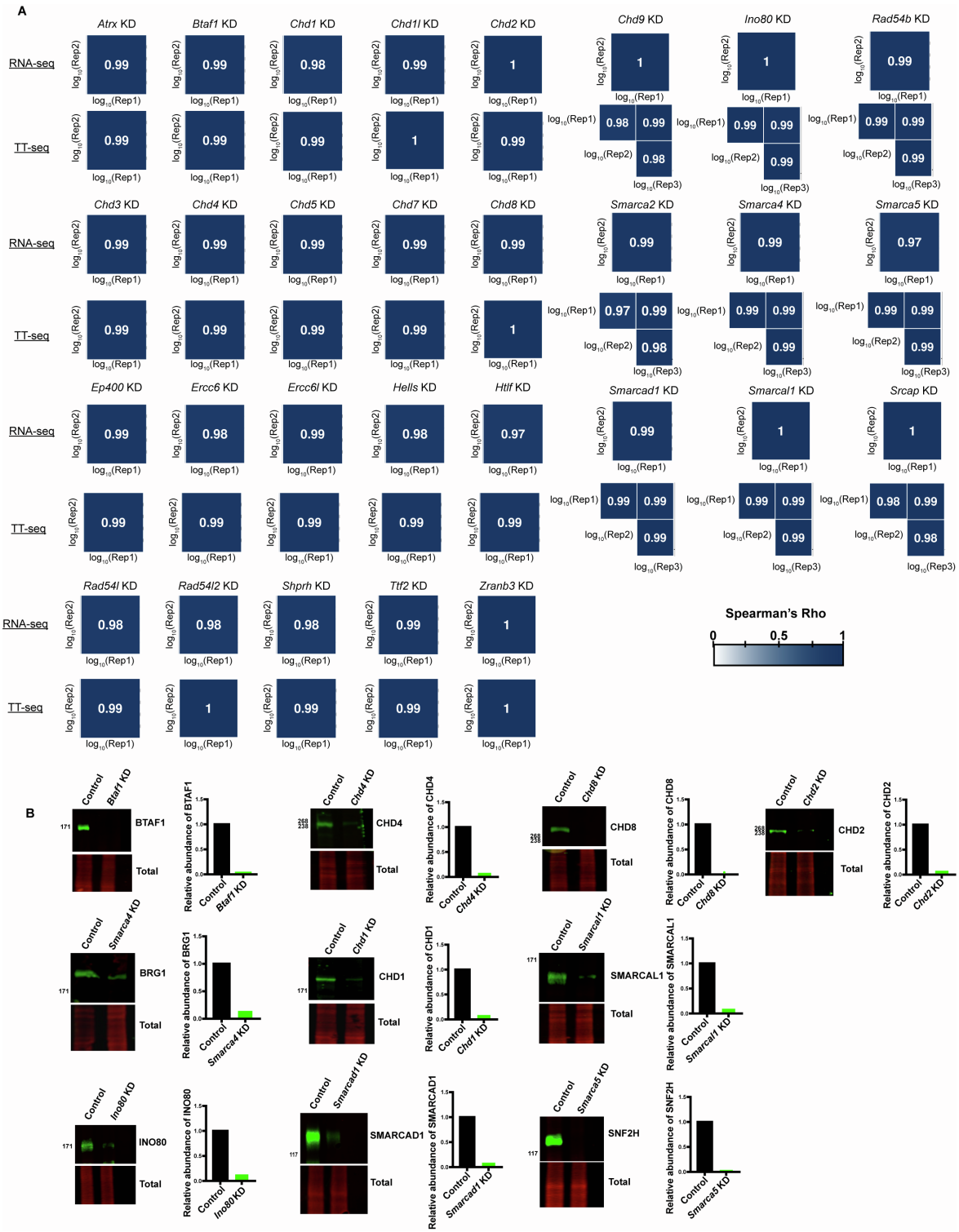

Figure S1: Reproducibility of TT-seq and RNA-seq replicates and remodeler depletion quality control. Related to Figures 1-4.

A. Heatmaps showing Spearman's correlation of $\log_{10}$(DEseq-normalized counts) of Gencode v23 features for biological replicates of each depletion condition in both TT-seq and RNA-seq datasets.

B. Western blots for 10 remodeler depletions.

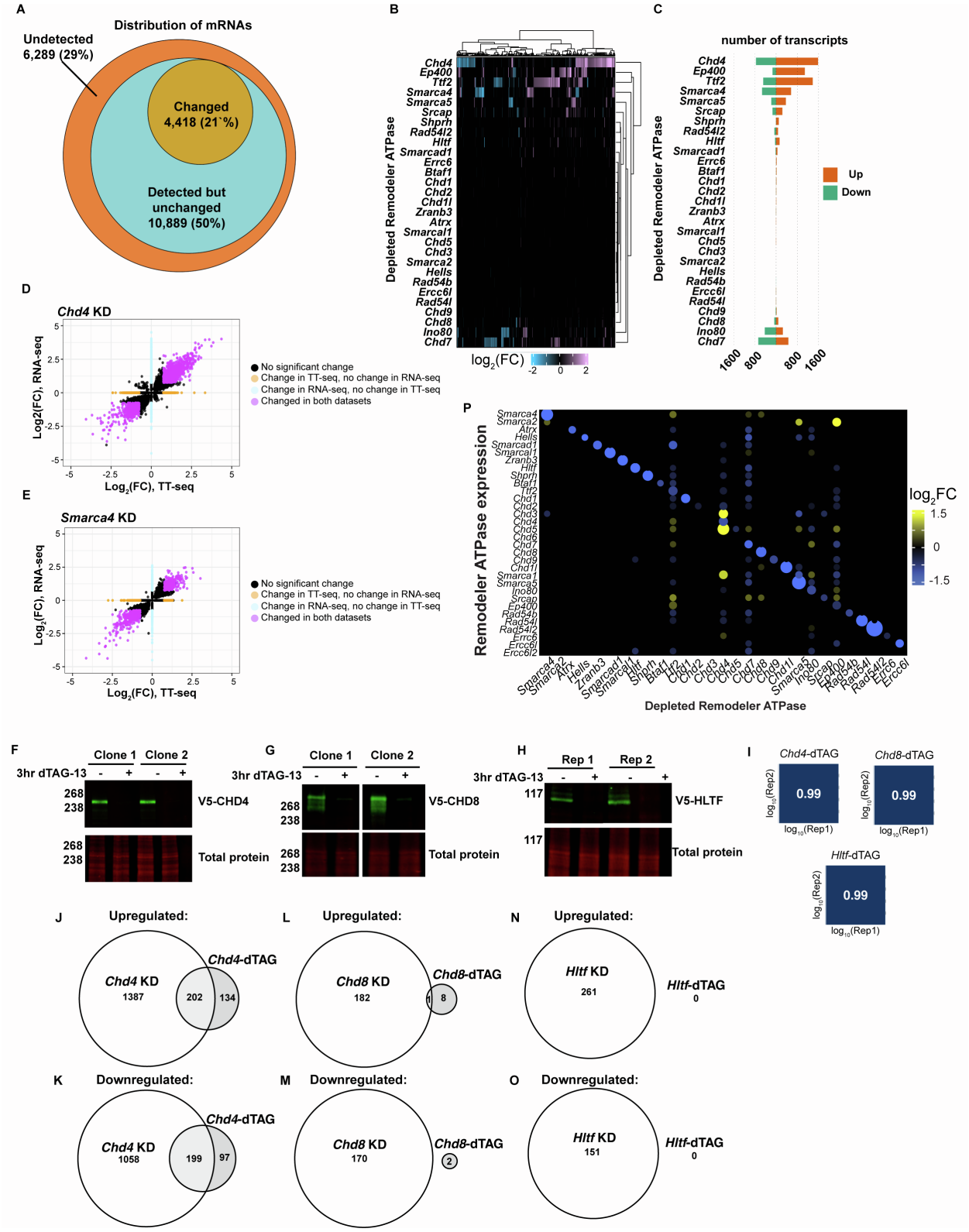

Figure S2: Remodeler depletions alter mRNA transcription throughout the ES cell genome. Related to Figure 1.

A. Venn diagram showing the distribution of mRNAs either undetected, detected but unchanged, or with changed transcription in this study, identified across all TT-seq datasets.
B. Heatmap showing the change in mRNA expression for genes changed across all 29 RNA-seq datasets ($|\log_2(FC)| \geq 0.75$ and FDR≤0.05). n=5,810 transcripts.
C. Barplot quantifying the number of mRNAs upregulated (orange) or downregulated (green) upon remodeler depletion using RNA-seq ($|\log_2(FC)| \geq 0.75$ and FDR≤0.05).
D. Scatterplot showing distribution of mRNAs with significant changes in transcription (TT-seq) and/or RNA-seq datasets for *Chd4* depletion ($|\log_2(FC)| \geq 0.75$ and FDR≤0.05). Purple dots represent mRNAs with correlated changes in both datasets, orange dots represent mRNAs with significant changes in TT-seq data only, blue dots represent mRNAs with significant changes in RNA-seq data only, and black dots represent mRNAs with not significant change in either dataset.
E. As in D, for *Smarca4* depletion.
F. Western blot for *Chd4*-dTAG cells treated with DMSO (-; vehicle) or dTAG (+) for 3 hours. Two independently generated clones are shown.
G. As in F, for *Chd8*-dTAG.
H. As in F, for two replicates of a single *Hltf*-dTAG clone.
I. Heatmaps showing Spearman's correlation of $\log_{10}$(DEseq-normalized counts) of Gencode v23 features for biological replicates of each depletion condition in TT-seq datasets.
J. Venn diagram showing number of upregulated mRNAs measured via TT-seq in *Chd4* KD (48 hour) vs *Chd4*-dTAG depletion (3 hour).
K. Venn diagram showing number of downregulated mRNAs measured via TT-seq in *Chd4* KD (48 hour) vs *Chd4*-dTAG depletion (3 hour).
L. As in J for *Chd8*.
M. As in K for *Chd8*.
N. As in J for *Hltf*.
O. As in K for *Hltf*.
P. Heatmap showing the change in mRNA expression (RNA-seq) of 32 ATPases (y-axis) upon individual depletion of 29 remodelers (x-axis; $|\log_2(FC)| \geq 0.75$ and FDR≤0.05). Dot size demonstrates significance.

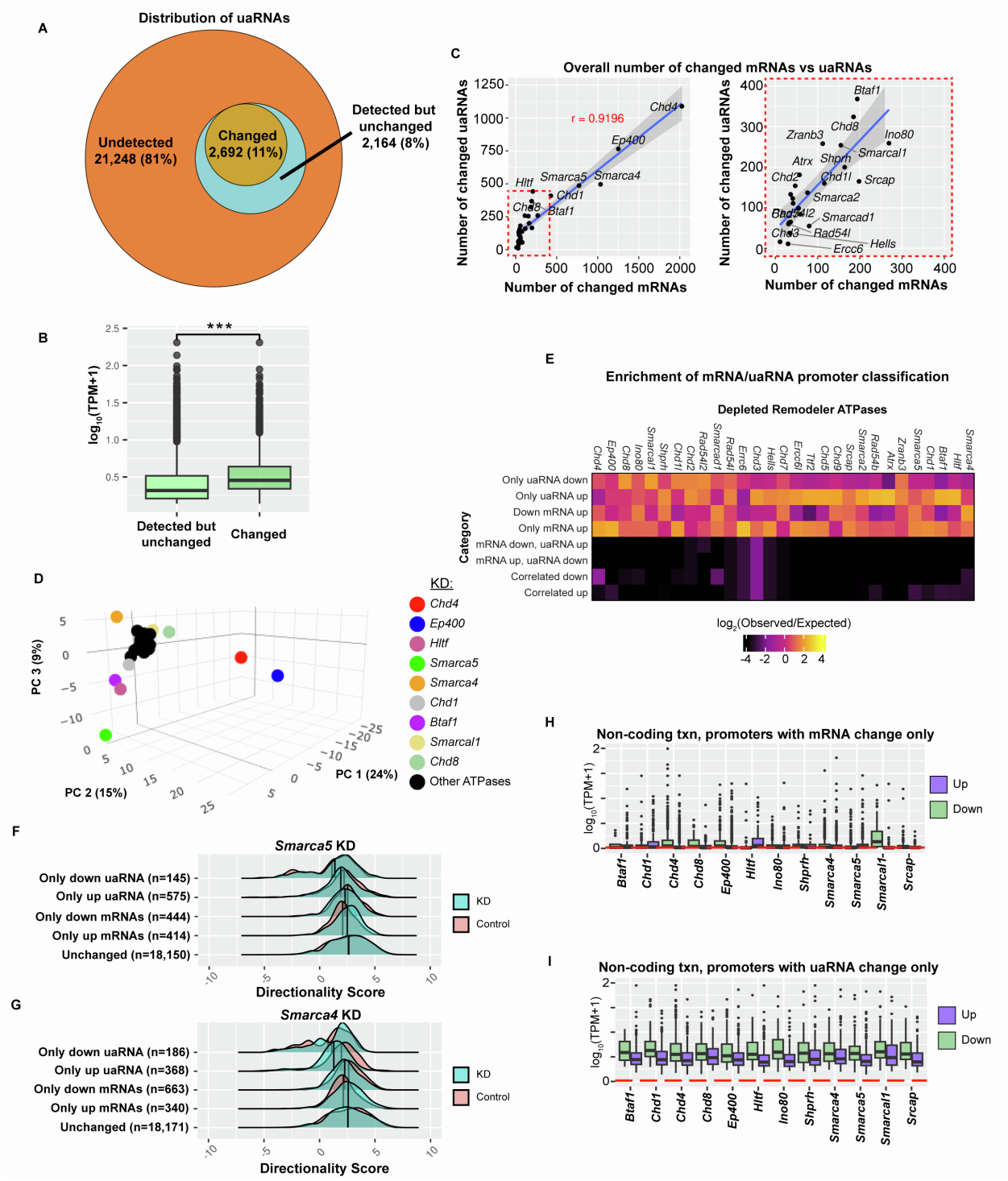

Figure S3: uaRNA transcription is regulated by many SNF2-type remodelers. Related to Figure 2 and 3.

A. Venn diagram showing the distribution of uaRNAs either undetected, detected but unchanged, or with changed transcription in this study, identified across all TT-seq datasets.

B. Boxplots comparing the relative transcription levels of uaRNAs with observable levels of transcription and significant changes in transcription (log_2(FC)≥0.5 and FDR≤0.05) in any depletion TT-seq dataset. The black line represents the median and edges represent the first and third quartiles.
C. Scatterplot comparing the numbers of mRNAs and uaRNAs with significant change in each depletion condition quantified using TT-seq. The right panel is a zoom-in containing the region outlined in the dotted red box in the left panel. mRNA change |log_2(FC)|≥0.75 and FDR≤0.05 and uaRNA change |log2(FC)|≥0.5 and FDR≤0.05.
D. PCA plot of differential transcription data from TT-seq where uaRNAs are changed in 3 or more depletions. n=1,307 transcripts.
E. Heatmap showing the ratio of observed over expected enrichment of promoters sorted into eight categories based on mRNA and uaRNA change in all depletions. *P*≤0.05, Chi-squared test of homogeneity assuming equal distribution across all categories. Yellow represents higher enrichment and black represents lower enrichment than expected.
F. Ridge plot comparing the directionality scores of promoters with significant changes in mRNA and/or uaRNA transcription from TT-seq in *Smarca5* depletion (blue) relative to control (pink). The black line represents the median value.
G. As in E, for *Smarca4* depletion.
H. Box plot quantifying wildtype ES cell uaRNA expression (TT-seq) at promoters showing only up (purple) or down (green) mRNA transcription in the indicated depletion.
I. As in J, for promoters showing only up or down uaRNA expression.

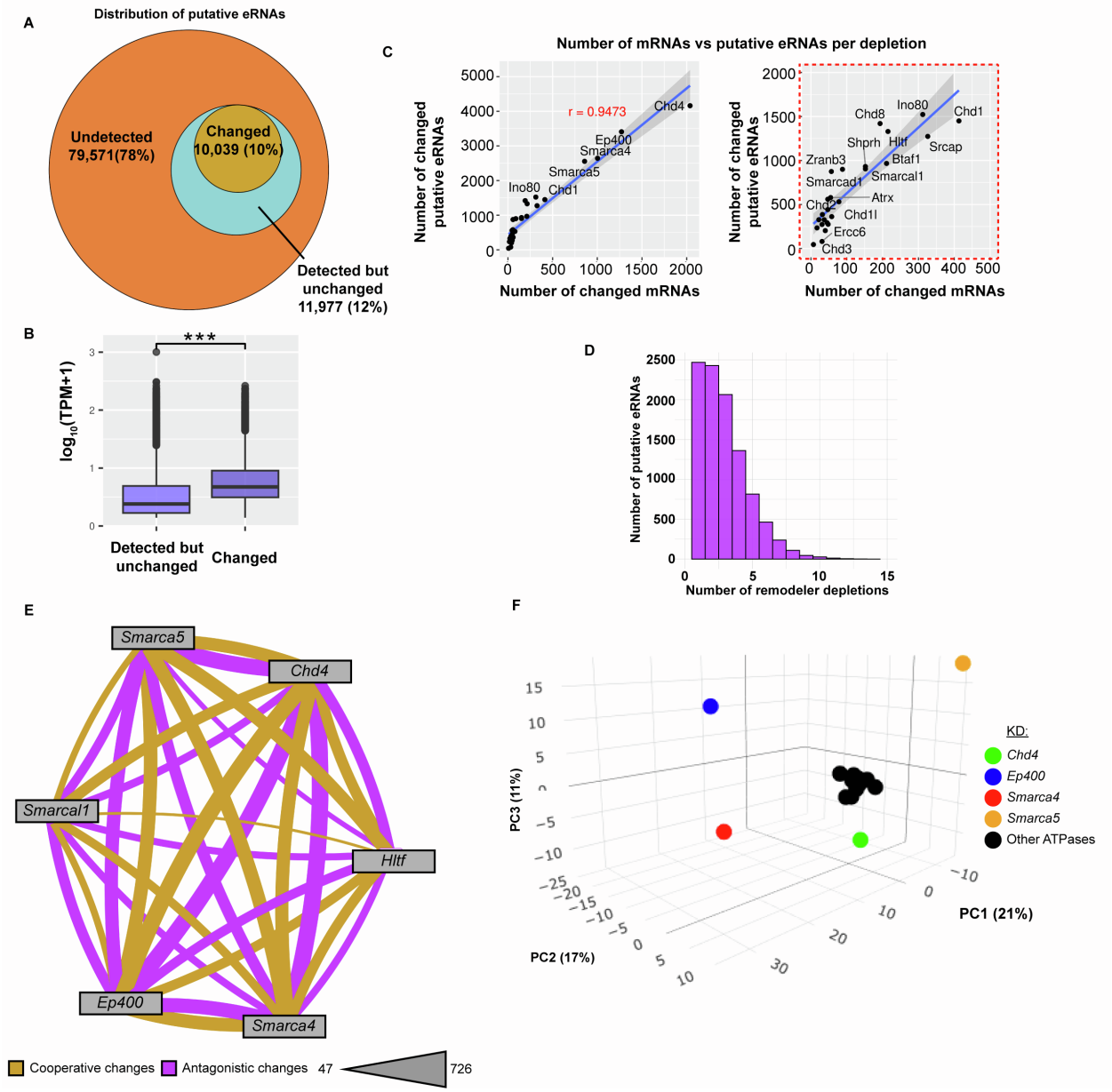

Figure S4: Many remodelers influence eRNA transcription in ES cells. Related to Figure 4.

A. Venn diagram showing the distribution of putative eRNAs either undetected, detected but unchanged, or with changed transcription in this study, identified across all TT-seq datasets.

B. Boxplots comparing the relative transcription levels of putative eRNAs with observable levels of transcription and significant changes in transcription (log_2(FC)≥0.5 and FDR≤0.05) in any depletion TT-seq dataset. The black line represents the median and edges represent the first and third quartiles.

C. Scatterplot comparing the numbers of mRNAs and putative eRNAs with significant changes in each depletion condition quantified using TT-seq. The right panel is a zoom in containing the region outlined in the dotted red box from the left panel. mRNA change

$|\log_2(FC)|\geq 0.75$ and FDR≤0.05 and putative enhancer change |log2(FC)|≥0.5 and FDR≤0.05. Spearman's rho=0.9473.

D. Histogram showing the distribution of putative eRNAs with altered transcription ($|\log_2(FC)|\geq 0.75$ and FDR≤0.05) in one or more depletion datasets quantified using TT-seq.
E. Network representing the number of putative eRNAs with altered transcription ($|\log_2(FC)|\geq 0.5$ and FDR≤0.05) in the same direction (cooperative, purple) or opposite direction (antagonistic, yellow) shared between six depletion datasets. Thickness of line correlates with number of putative enhancers in category shared between datasets, with the range listed.
F. PCA plot of differential transcription data from TT-seq where putative eRNAs are changed in 3 or more depletions. N=5,143 transcripts.

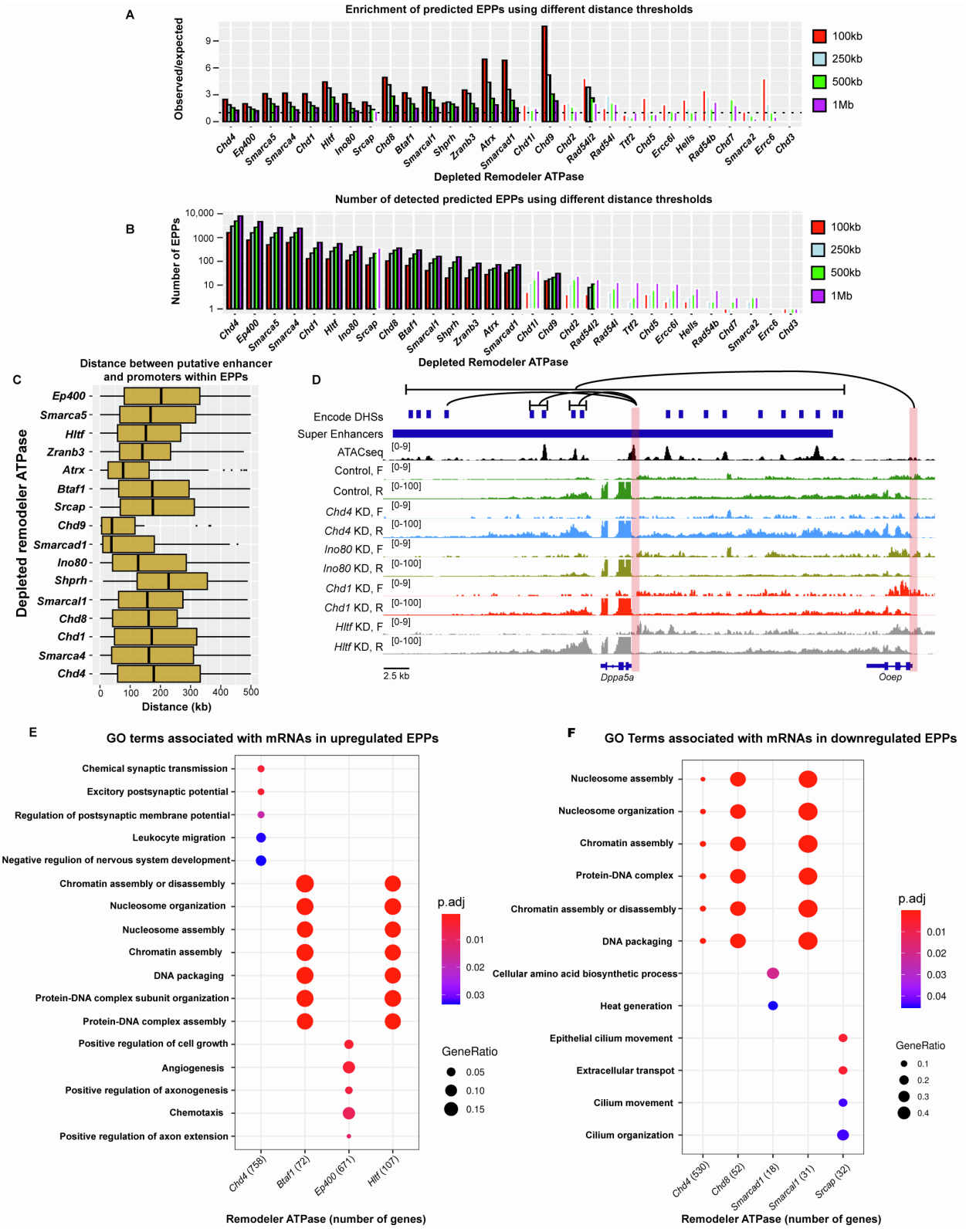

Figure S5: Characterization of EPPs detected in 16 remodeler depletions. Related to Figure 4.

A. Barplot showing the ratio of observed predicted enhancer-promoter pairs (EPPs) in each depletion using different distance thresholds over expected numbers determined by permutation test (n=1,000). Bars with black outlines represent observed numbers significantly different from expected numbers determined by permutation test (Benjamini & Yekutieli Adjusted *P* value≤0.05). TT-seq.
B. Barplot showing the number of predicted EPPs in each depletion quantified with TT-seq using different distance thresholds. Bars with black outlines represent observed numbers significantly different from expected numbers determined by permutation test (Benjamini & Yekutieli Adjusted *P* value≤0.05).
C. Boxplots representing the distribution of distances between predicted EPPs in each depletion using a 500 kB distance threshold. The black line represents the median and edges represent the first and third quartiles.
D. Browser track showing chromatin accessibility (ATAC-seq) and comparing transcription (TT-seq) in the control, *Chd4* KD, *Ino80* KD, *Chd1* KD, and *Hltf* KD over the *Dppa5a* locus, *Ooep* locus, and the interacting nearby super enhancer region. Red boxes indicate promoter regions of each locus, and lines indicate DHSs within the super enhancer region shown to interact with each promoter.
E. GO terms associated with mRNAs in predicted upregulated EPPs in *Chd4*, *Btaf1*, *Ep400*, and *Hltf* depletions quantified using TT-seq. Number in parenthesis indicates the number of mRNAs in predicted upregulated EPPs in that depletion. Size of dot indicates relative proportion of total mRNAs associated with indicated GO term and color indicates significance of the association.
F. As in D, for GO terms associated with mRNAs in predicted downregulated EPPs in *Chd4*, *Chd8*, *Smarcad1*, *Smarcal1*, and *Srcap* depletions.

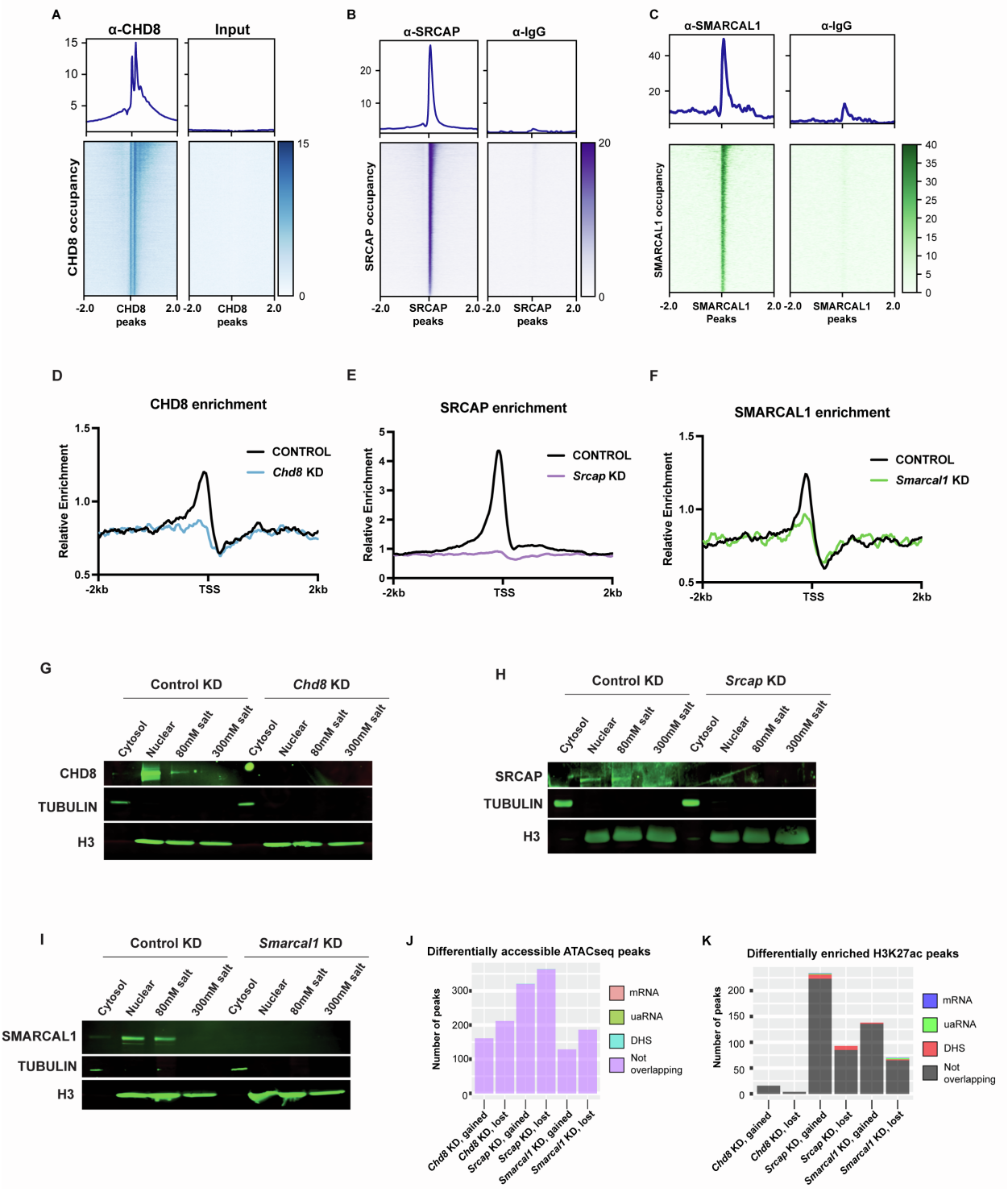

Figure S6: Chromatin binding for CHD8, SRCAP, and SMARCAL1. Related to Figures 5-7.

A. Heatmap showing the enrichment of CHD8 binding over called peaks relative to input from available ChIP-seq data (GSE64825). n=30,053 peaks.

B. Heatmap showing SRCAP binding over called peaks relative to IgG using CUT&RUN. n=50,743 peaks.

C. Heatmap showing SMARCAL1 binding over called peaks relative to IgG using CUT&RUN. n= 2,271 peaks.
D. Metaplot showing enrichment of CHD8 binding over transcription start sites (TSSs) in control vs *Chd8* KD using CUT&RUN.
E. Metaplot showing enrichment of SRCAP binding over TSSs in control vs *Srcap* KD using CUT&RUN.
F. Metaplot showing enrichment of SMARCAL1 binding over TSSs in control vs *Smarcal1* KD using CUT&RUN.
G. Chromatin salt fractionation using control and *Chd8* KD. Tubulin acts as a cytosolic control and H3 acts as a nuclear control. CHD8 is observed in the nuclear and 80mM salt fraction, but absent in all *Chd8* KD fractions.
H. As in G, for *Srcap* KD.
I. As in G, for *Smarcal1* KD.
J. Barplot showing the number of ATAC-seq peaks with differential accessibility ($|\log_2(FC)| \geq 0.5$ and FDR≤0.05) in *Chd8*, *Srcap*, or *Smarcal1* depletions, and the number of peaks that overlap promoters or enhancers with correlated significant changes in mRNA, uaRNA, or putative eRNA transcription quantified with TT-seq.
K. Barplot showing the number of H3K27ac CUT&RUN peaks with differential enrichment ($|\log_2(FC)| \geq 0.5$ and FDR≤0.05) in *Chd8*, *Srcap*, or *Smarcal1* depletions, and the number of peaks that overlap promoters or enhancers with correlated significant changes in mRNA, uaRNA, or putative eRNA transcription quantified with TT-seq.

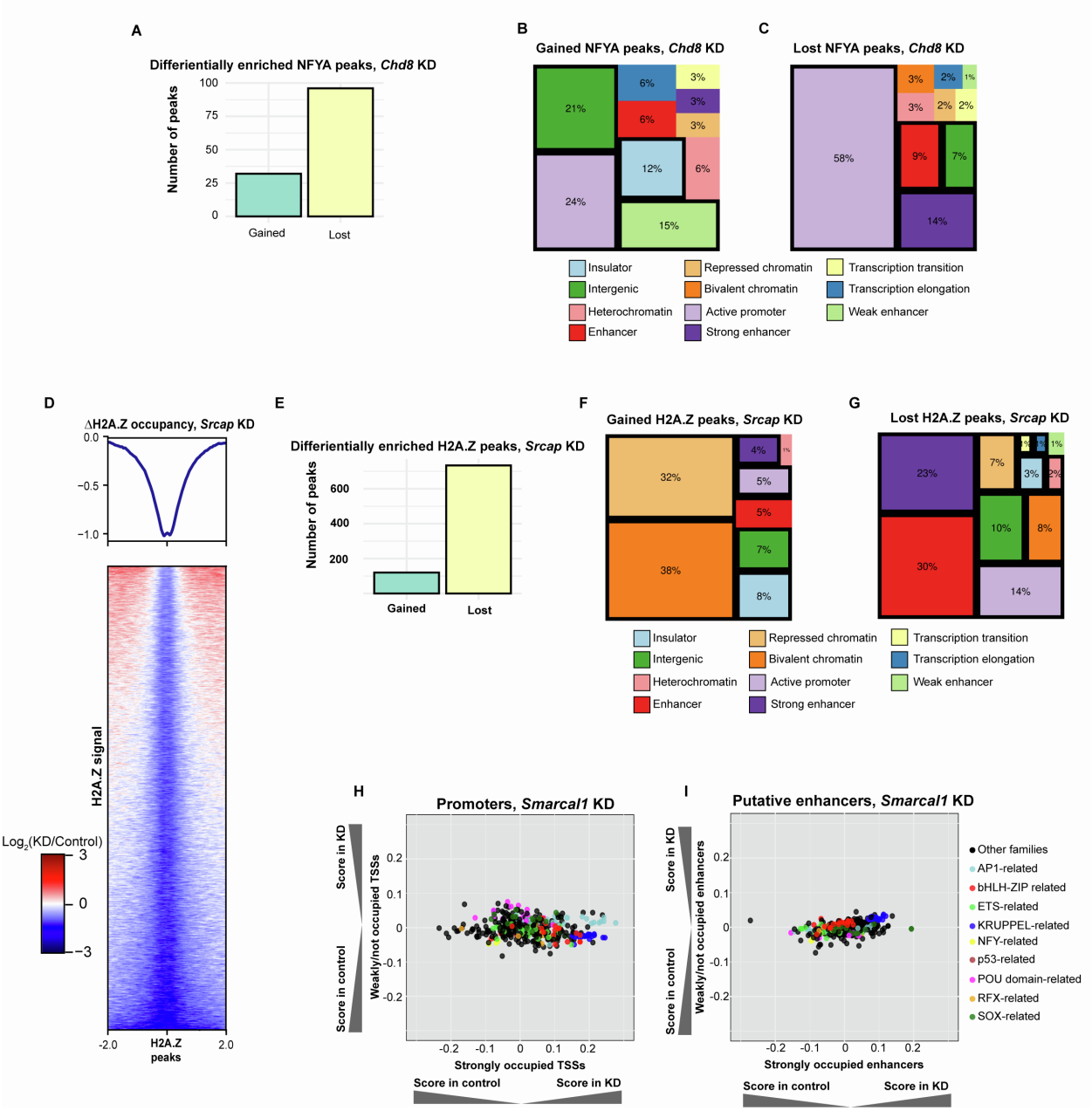

Figure S7: Characterization of chromatin changes upon depletion of *Chd8*, *Srcap*, or *Smarcal1* in ES cells. Related to Figures 5-7.

A. Barplot showing the number of gained or lost differentially enriched NFYA CUT&RUN peaks in *Chd8* depletion relative to control. $\log_2$(FC)≥0.5 and FDR≤0.05
B. Treemap showing the distribution of chromatin states (defined by ChromHMM) that overlap with NFYA gained CUT&RUN peaks in the *Chd8* depletion. Relative size and percentage represent the fraction of total peaks overlapping each chromatin state. States outlined in black represent significantly enriched categories (Fisher's test, Bonferroni adjusted P value ≤0.05).
C. As in B, for NFYA CUT&RUN peaks lost upon *Chd8* depletion.
D. Heatmap showing the change in H2A.Z binding over called H2A.Z peaks in the *Srcap* KD relative to control CUT&RUN experiments. n=29,950 peaks.

E. As in A, for gained and lost H2A.Z CUT&RUN peaks upon *Srcap* depletion.
F. As in B, for H2A.Z CUT&RUN peaks gained upon *Srcap* depletion.
G. As in B, for H2A.Z CUT&RUN peaks lost upon *Srcap* depletion.
H. Scatterplot comparing the binding score of different transcription factor motifs at promoters bound versus not bound by SMARCAL1. Motifs representing factors from similar related groups are colored according to the legend. All factors shown have $P \leq 0.05$ at bound and unbound loci, defined from ATAC-seq data using TOBIAS.
I. As in L, for putative enhancers bound by SMARCAL1.